Non-uniqueness of the Quasinormal Mode Expansion of Electromagnetic Lorentz Dispersive Materials

Marc Duruflé, Alexandre Gras, Philippe Lalanne

Non-uniqueness of the Quasinormal Mode Expansion of Electromagnetic Lorentz Dispersive Materials

Marc Duruflé, Alexandre Gras, Philippe Lalanne

RESEARCH REPORT
N° 9348
June 2020
Project-Team Magique-3D

ISSN 0249-6399 ISRN INRIA/RR--9348--FR+ENG

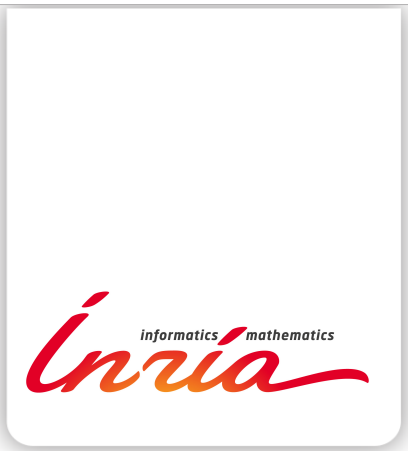

Non-uniqueness of the Quasinormal Mode Expansion of Electromagnetic Lorentz Dispersive Materials

Marc Duruflé*, Alexandre Gras*†, Philippe Lalanne†

Project-Team Magique-3D

Research Report n° 9348 — June 2020 — 45 pages

Abstract: Any optical structure possesses resonance modes and its response to an excitation can be decomposed onto the quasinormal and numerical modes of discretized Maxwell's operator. In this report, we consider a dielectric permittivity that is a N-pole meromorphic function of the pulsation ω (Lorentz model). We propose a common formalism and obtain different formulas for the modal expansion. The non-uniqueness of the excitation coefficient is due to a choice of the linearization of Maxwell's equation with respect to ω and of the form of the source term. We make the link between the numerical discrete modal expansion and analytical formulas that can be found in the literature. We detail the formulation of dispersive Perfectly Matched Layers (PML) in order to keep a linear eigenvalue problem. We also give an algorithm to regain an orthogonal basis for degenerate modes. Numerical results validate the different formulas and compare their accuracy.

Key-words: electromagnetic resonance, quasinormal mode, microcavity, nanoresonator, modal expansion

* Institute of Mathematics of Bordeaux, INRIA Bordeaux Sud-Ouest, EPI Magique 3-D
† LP2N, Institut d'Optique Graduate School, CNRS, Univ. Bordeaux

RESEARCH CENTRE BORDEAUX – SUD-OUEST

200 avenue de la Vieille Tour
33405 Talence Cedex

Non-unicité de la décomposition en modes quasi-normaux d'un champ électromagnétique pour des matériaux dispersifs régis par le modèle de Lorentz

Résumé : Un dispositif optique possède des modes de résonances et sa réponse à une excitation peut être décomposée sur les modes quasi-normaux et les modes numériques de l'opérateur de Maxwell discrétisé. Dans ce papier, on considère une permittivité diélectrique qui est une fonction méromorphe de ω avec N pôles (modèle de Lorentz). Nous proposons un formalisme géneral pour obtenir différentes formules pour la décomposition selon les modes. La non-unicité du coefficient d'excitation est dû au choix de la linéarisation des équations de Maxwell par rapport à ω et de la forme du terme source. Nous établissons le lien entre la décomposition modale discrète et des formules analytiques qui peuvent être trouveées dans la littérature. Nous détaillons la formulation avec des PML (Perfectly Matched Layers) dispersives afin de conserver un problème aux valeurs propres linéaire. Nous donnons aussi un algorithme pour retrouver une base orthogonale pour les modes dégénérés. Des résultats numériques valident les différentes formules et comparent leur précision.

Mots-clés : résonance électromagnétique, mode quasi-normale, microcavité, nano-résonateur, décomposition modale

Contents

1 Introduction

1.1 Quasinormal Modes

Optical micro and nanoresonators, be they plasmonic, photonic or hybrid, enhance and localize the electromagnetic energy at wavelength or subwavelength scales and are key components in many photonic applications. Their optical response is characterized by one of a few resonant

features resulting from the excitation of one or a few dominant modes, the natural resonance modes of the resonators. These modes conveniently labelled by the integer $m = 1, 2...$ are characterized by their electric and magnetic field vectors distributions, $\mathbf{E}_m(\mathbf{r})$ and $\mathbf{H}_m(\mathbf{r})$. These vectors are solutions of the following eigenvalue boundary problem (Lalanne et al., 2018)

$$\begin{cases} -i\,\tilde{\omega}_m \varepsilon(\tilde{\omega}_m)\mathbf{E}_m - \nabla \times \mathbf{H}_m &= 0, \\ -i\,\tilde{\omega}_m \mu(\tilde{\omega}_m)\mathbf{H}_m + \nabla \times \mathbf{E}_m &= 0, \\ + \text{ Boundary conditions} \end{cases} \tag{1}$$

where $\varepsilon(\omega)$ and $\mu(\omega)$ are respectively the dielectric permittivity and magnetic permeability and depend on the position $\mathbf{r}$ and pulsation ω. The $\exp(-i\omega t)$ convention for time harmonic fields is assumed. The fields $\mathbf{E}_m(\mathbf{r})$ have continuous tangent traces across interfaces between subdomains and satisfy the outgoing-wave conditions at infinity. They are often called quasinormal modes (QNMs) to emphasize that their harmonic evolution is characterized by an exponential damping in time (they are the eigenstates of a non-Hermitian operator), so to say their pulsation $\tilde{\omega}_m$ is complex with $\mathrm{Im}(\tilde{\omega}_m) < 0$. Micro and nanoresonators play a leading role in many areas in nanophotonics, from quantum information processing to ultrasensitive biosensing, nonlinear optics, and various optical metasurfaces. This pushes a strong pressure on the development of QNM theory and QNM numerical methods that explicitly consider QNMs in the analysis, providing important clues towards the interpretation of the resonator response.

1.2 Quasinormal Mode expansion of the scattered field

The scattered field $[\mathbf{E}_S(\mathbf{r},\omega), \mathbf{H}_S(\mathbf{r},\omega)]$ is solution of time-harmonic Maxwell's equations

$$\begin{cases} -i\,\omega\,\varepsilon(\omega)\mathbf{E}_S - \nabla \times \mathbf{H}_S &= i\omega(\varepsilon(\omega) - \varepsilon_b)\,\mathbf{E}_{\text{inc}}, \\ -i\,\omega\,\mu(\omega)\mathbf{H}_S + \nabla \times \mathbf{E}_S &= i\omega(\mu(\omega) - \mu_b)\mathbf{H}_{\text{inc}}, \\ + \text{ Sommerfeld condition}, \end{cases}$$

where $\mathbf{E}_{\text{inc}}, \mathbf{H}_{\text{inc}}$ is the incident field, and ε_b, μ_b the background indices. The incident fields $\mathbf{E}_{\text{inc}}, \mathbf{H}_{\text{inc}}$ satisfy homogeneous Maxwell's equations with indices ε_b, μ_b. Let us introduce

$$\mathbf{J} = i\omega(\varepsilon(\omega) - \varepsilon_b)\,\mathbf{E}_{\text{inc}}$$

and we consider only non-ferromagnetic media such that $\mu(\omega) = \mu_b = \mu_0$ in the physical domain. As a result, the Maxwell's equations that will considered in the sequel are given as

$$\begin{cases} -i\,\omega\,\varepsilon(\omega)\mathbf{E}_S - \nabla \times \mathbf{H}_S &= \mathbf{J}, \\ -i\,\omega\,\mu(\omega)\mathbf{H}_S + \nabla \times \mathbf{E}_S &= 0, \\ + \text{ Sommerfeld condition }. \end{cases} \tag{2}$$

Efficiently computing this scattered field for a large number of pulsations consists in expanding the solution into the QNM basis :

$$\mathbf{E}_S(\mathbf{r},\omega) = \sum_m \alpha_m(\omega)\mathbf{E}_m(\mathbf{r},\omega),$$

where the α_m's are the complex modal excitation coefficients, which measure how much the QNMs are excited by the driving field illuminating the resonator with a real frequency ω.

There are still some complicated mathematical issues in relation with the actual physical problem for which the open space is infinite and Maxwell's operator are continuous. For instance, the conditions under which the completeness of the QNM expansions of Eq. (1) is guaranteed are not still fully understood (Colom et al., 2018; Abdelrahman and Gralak, 2018). There are also several known and correct expressions for the α_m's (Lalanne et al., 2018), but we do not know which offer the best performance, e.g. the fastest convergence rate towards the actual solution as the number of QNMs retained in the expansion increases.

However, for practical geometries of interest in nanophotonics, the QNMs are computed numerically and it would be unrealistic to expect computing many QNMs over a broad spectral range, ideally in the entire lower half-plane of the complex plane ($\mathrm{Im}(\tilde{\omega}_m) < 0$). Rather we have to consider a discretized version of the initial Maxwell's equations and the physical domain is bounded by perfectly-matched layers (PMLs). The discretized operator is a matrix of finite dimension, and its spectrum is composed of a finite number of QNMs (often the relevant ones involved in the resonator dynamics in the spectral range of interest) completed by a large number of PML modes, which have much less physical significance but warrant completeness (Vial et al., 2014; Yan et al., 2018; Lalanne et al., 2018).

Efficient QNMs solvers exist for computing and normalizing QNMs and PML modes for various geometries, such as plasmonic crystals, metal gratings and plasmonic nanoantennas (Lalanne et al., 2019); even freeware (Bai et al., 2013) or improved commercial software packages (Yan et al., 2018) can be used. Thus the important remaining step is the reconstruction problem, i.e. the computation of the modal coefficients α_m's and the reconstruction of the scattered field.

While the concept of the QNM expansion as described by equation (1) is a common feature among papers on modal expansions, the expression of the excitation coefficient α_m changes depending on the method used to project the scattered field onto the QNM basis. The contour integral method described in (Binkowski et al., 2019; Zschiedrich et al., 2018) necessitates an integration path in the complex frequency plane which encloses the eigenmodes of interests. The scattered field at the real frequency can thus be expressed as a sum of two contributions : a resonant contribution made up of contour integrals around the eigenfrequencies in the complex plane, and a non-resonant contribution, a setup that's echoed in (Colom et al., 2018).

There also exists the resonant state expansion method described in (Muljarov and Langbein, 2016) where the modal expansion is obtained from the decomposition of the Green's function in QNMs. For dispersive materials whose permittivity can be described with a Drude model, the auxiliary field method and biorthogonal relations (Yan et al., 2018) can be used to derive an analytical expression of α_m. An improved formula for the field inside the resonator has been obtained in Wu et al. (2019). For the same material permittivity, however, another formula for α_m was found in (Zolla et al., 2018), without the use of auxiliary fields. Finally, we can cite also (Zimmerling et al., 2016), where the eigenmodes are solved simultaneously with the reconstruction, such that only significant eigenmodes are kept.

This report will focus on the reconstruction problem of resonators composed of Drude-Lorentz materials. For these cases, we wish to make explicit possible sources of the non-uniqueness of the expressions of the excitation coefficients α_m by using a common formalism. This common formalism is based on a discrete version of Maxwell's equations, which we will use to derive the different formulas. It was important for us to obtain these formulas from a discrete point of view in order to ensure that the numerical modal expansion converges indeed towards the expected solution. It will be shown that different linearizations of the nonlinear eigenvalue problem with the use of auxiliary fields yield different formulas of α_m. With this approach, already known formulas are found. Furthermore, we show that an infinity of formulas can be derived easily by choosing appropriate source terms. Numerical results will show that the tested formulas converge towards the same reference solution. It will also be explained how degenerate eigenvalues (i.e.

multiple eigenvalues) can be treated correctly with a simple Gram-Schmidt orthogonalization procedure.

In section 2, the Lorentz model used for the dielectric permittivity is detailed and the common formalism used to obtain different formulas for α_m is introduced. In the sections 3 and 4.3, two different linearizations of Maxwell's equation are detailed providing different formulas of α_m. The computational domain has to be truncated, e.g. with Perfectly Matched Layers. In order to keep a real eigenvalue problem, we have chosen to implement dispersive PMLs, that are detailed in subsection 4.6. Finally, numerical results are presented in section 5 in order to compare the accuracy of the different formulas that will have been rederived.

2 General setting

2.1 Drude-Lorentz model for the permittivity

The dielectric permittivity depends on the pulsation ω and can be approximated efficiently with Padé approximant, which usually necessitates a lower degree than a simple polynomial approximation. Assuming that all poles of the Padé approximation are simple (see (Sehmi et al., 2017b)), we can approximate the permittivity as

$$\varepsilon(\omega) = \sum_{k=1}^{L} \frac{i\sigma_k}{\omega - \Omega_k}$$

where Ω_k are poles in the half complex plane ($\mathrm{Im}(\Omega_k) < 0$), σ_k are complex coefficients and L is the number of poles. However, this first approximation is not physically relevant since it does not respect the causality principle that requires that:

$$\bar{\varepsilon}(\omega) = \varepsilon(-\bar{\omega})$$

where $\bar{\omega}$ denotes the conjugate of ω. Therefore, a physically relevant approximation is the following one (see for instance (Sehmi et al., 2017b))

$$\varepsilon(\omega) = \varepsilon_\infty + \sum_{d=1}^{D} \frac{i\eta_k}{\omega + i\tilde{\gamma}_k} + \sum_{k=1}^{L} \left(\frac{i\sigma_k}{\omega - \Omega_k} + \frac{i\bar{\sigma}_k}{\omega + \bar{\Omega}_k} \right) \tag{3}$$

where σ_k and Ω_k are complex coefficients and $\tilde{\gamma}_k, \eta_k$ are real coefficients. We assume that $\mathrm{Im}(\omega_k) < 0$ and $\tilde{\gamma}_k > 0$ such that all the poles of $\varepsilon(\omega)$ are located in the half complex plane $\mathrm{Im}(z) < 0$. For the last sum of (3), we can reduce to the same denominator to obtain

$$\frac{i\sigma_k}{\omega - \Omega_k} + \frac{i\bar{\sigma}_k}{\omega + \bar{\Omega}_k} = -\frac{c_k - i\omega\tilde{\sigma}_k}{\omega^2 - \omega_{0,k}^2 + i\gamma_k\omega}$$

with the relations

$$\omega_{0,k} = |\Omega_k|,\ \gamma_k = -2\mathrm{Im}(\Omega_k),\ \tilde{\sigma}_k = 2Re(\sigma_k),\ c_k = 2\mathrm{Im}\left(\sigma_k\bar{\Omega}_k\right).$$

The constants $\omega_{0,k}, \gamma_k, \tilde{\sigma}_k$ and c_k are real. For the first sum of (3), if we consider an even number D, we can regroup terms two by two:

$$\frac{i\eta_k}{\omega + i\tilde{\gamma}_k} + \frac{i\eta_{k+1}}{\omega + i\tilde{\gamma}_{k+1}} = -\frac{c_k - i\omega\tilde{\sigma}_k}{\omega^2 - \omega_{0,k}^2 + i\gamma_k\omega}$$

with the relations

$$\omega_{0,k} = \sqrt{\tilde{\gamma}_k \tilde{\gamma}_{k+1}},\ \gamma_k = \tilde{\gamma}_k + \tilde{\gamma}_{k+1},\ \tilde{\sigma}_k = \eta_k + \eta_{k+1},\ c_k = \eta_k \tilde{\gamma}_{k+1} + \eta_{k+1}\tilde{\gamma}_k$$

Again, the constants $\omega_{0,k}, \gamma_k, \tilde{\sigma}_k$ and c_k are real. For metallic materials, good approximations are obtained by choosing $D = 2$ (see Sehmi et al. (2017b)). For other materials, we can take $D = 0$ (see (Sehmi et al., 2017a)). As a result, we will consider the following model of permittivity

$$\varepsilon(\omega) = \varepsilon_\infty - \sum_{k=1}^{L} \frac{c_k - i\omega\sigma_k}{\omega^2 - \omega_{0,k}^2 + i\gamma_k\omega}, \tag{4}$$

with real coefficients $c_k,\ \sigma_k,\ \omega_{0,k}, \gamma_k$. This model can also be obtained by considering the motion of electrons (see (Wooten, 1972)) for which we have $\sigma_k = 0$.

2.2 Discrete modal expansion

For a Drude-Lorentz model (as described in the previous sub-section) of $\varepsilon(\omega)$, auxiliary unknowns can be introduced in order to obtain a linear eigenvalue problem. After this linearization procedure and after discretization (e.g. with Finite Element Method), the time-harmonic Maxwell's Equations can be written

$$-i\omega\mathbf{M}_h\mathbf{U}_h + \mathbf{K}_h\mathbf{U}_h = \mathbf{F}_h, \tag{5}$$

where $\mathbf{M}_h$ is the mass matrix, $\mathbf{K}_h$ is the stiffness matrix, and $\mathbf{F}_h$ is the source term (h denotes the mesh size). $\mathbf{U}_h$ is the main unknown that will contain components of $\mathbf{E}$ and other auxiliary unknowns introduced to obtain a linear eigenvalue problem. The matrices $\mathbf{M}_h$ and $\mathbf{K}_h$ are real and independent of ω, an example of matrices will be given in section 3. The right eigenvectors $\mathbf{x}_m$ and left eigenvectors $\mathbf{x}_m^\perp$ solve the following linear eigenvalue problems which are transposed from each other

$$\mathbf{K}_h\mathbf{x}_m = i\tilde{\omega}_m\mathbf{M}_h\mathbf{x}_m, \quad \mathbf{K}_h^T\mathbf{x}_m^\perp = i\tilde{\omega}_m\mathbf{M}_h^T\mathbf{x}_m^\perp.$$

From a discrete point of view, once the discrete linear system (5) is set, the biorthogonal projection of the unknown $\mathbf{U}_h$ provides an unique formula for α_m:

$$\alpha_m = \frac{1}{i(\tilde{\omega}_m - \omega)}\langle \mathbf{F}_h, \mathbf{x}_m^\perp \rangle, \tag{6}$$

This biorthogonal projection is obtained by considering the relation (5) and taking the scalar product with the left eigenvector $\mathbf{x}_m^\perp$. In this document, the convention $\langle x, y\rangle = \sum x_i y_i$ is used (without conjugate). Because Maxwell's equations usually provide a complex symmetric linear system for the unknown $\mathbf{E}_h$ (when other unknowns are substituted), the left eigenvector can be computed directly from the right eigenvector. The expressions will be given for the different linearizations introduced. The formula (6) holds if the left and right eigenvectors $\mathbf{x}_m, \mathbf{x}_m^\perp$ are normalized such that

$$\langle \mathbf{M}_h\mathbf{x}_m, \mathbf{x}_m^\perp \rangle = 1. \tag{7}$$

As detailed in section 3, the discrete relation (6) can be rewritten with integrals in order to obtain analytic formulas for α_m. With this procedure, we have obtained the following formulas (already known in the literature)

- The formula 5.11 in Lalanne et al. (2018):

$$\alpha_m = \frac{1}{i(\tilde{\omega}_m - \omega)} \int_{\Omega_{res}} \mathbf{J}(\mathbf{r}) \cdot \mathbf{E}_m(\mathbf{r}) d\mathbf{r} \tag{8}$$

  which is obtained by a direct linearization of the system (2) (detailed in section 3).

- The formula proposed in Yan et al. (2018) (equivalent to formula 5.6 in Lalanne et al. (2018)):

$$\alpha_m = \int_{\Omega_{res}} (\varepsilon_b - \varepsilon_\infty)\mathbf{E}_{inc} \cdot \mathbf{E}_m d\Omega + \frac{\tilde{\omega}_m}{\tilde{\omega}_m - \omega} \int_{\Omega_{res}} (\varepsilon(\tilde{\omega}_m) - \varepsilon_b)\mathbf{E}_{inc} \cdot \mathbf{E}_m d\Omega \tag{9}$$

  which is obtained by choosing a different source $\mathbf{F}_h$ (detailed in section 4.1).

- The formula proposed in Zolla et al. (2018) (equivalent to formula 5.10 in Lalanne et al. (2018)):

$$\alpha_m = \frac{\omega}{i\,\tilde{\omega}_m(\tilde{\omega}_m - \omega)} \int_{\Omega_{res}} \mathbf{J}(\mathbf{r}) \cdot \mathbf{E}_m(\mathbf{r})\, d\mathbf{r} \tag{10}$$

  which is obtained by starting from the second-order formulation of Maxwell's equations with curl-curl operator (detailed in section 4.3).

In these formulas, Ω_{res} denotes the domain of the resonator for which $\varepsilon(\omega)$ is different from ε_b (hence it is the support of the source term $\mathbf{J}$). All these formulas hold if the modes $\mathbf{E}_m$ are normalized as follows

$$\int_\Omega \frac{\partial(\tilde{\omega}_m\, \varepsilon(\tilde{\omega}_m))}{\partial\tilde{\omega}_m}\mathbf{E}_m \cdot \mathbf{E}_m - \frac{\partial\,(\tilde{\omega}_m \mu(\tilde{\omega}_m))}{\partial\tilde{\omega_m}}\,\mathbf{H}_m \cdot \mathbf{H}_m d\Omega = 1. \tag{11}$$

where Ω is the computational domain. This is the usual normalization Muljarov and Langbein (2016); Sauvan et al. (2013); Bai et al. (2013). An infinite set of formulas can be found by splitting the source on the different fields. For the linearization given in section 3, by writing the generalized source term as $\mathbf{F} = [\mathbf{f}_1, \mathbf{f}_2, \mathbf{f}_{3,k}, \mathbf{f}_{4,k}]$, we can find the following generalization of the modal excitation coefficient:

$$\alpha_m = \frac{1}{i(\omega_m - \omega)} \int_{\Omega_{res}} \mathbf{f}_1 \cdot \mathbf{E}_m - \mathbf{f}_2 \cdot \mathbf{H}_m + \left(\sum_{k=1}^{L} \frac{\left(\omega_{0,k}^2 \mathbf{f}_{3,k} + i\tilde{\omega}_m \mathbf{f}_{4,k}\right)}{-\tilde{\omega}_m^2 + \omega_{0,k}^2 - i\gamma_k\tilde{\omega}_m} \cdot \mathbf{E}_m \right) d\Omega_{res} \tag{12}$$

provided that

$$\mathbf{f}_1 + \left(\sum_{k=1}^{L} \frac{i\omega\mathbf{f}_{4,k} + \omega_{0,k}^2 \mathbf{f}_{3,k}}{-\omega^2 - i\omega\gamma_k + \omega_{0,k}^2} \right) + \frac{i}{\omega}\nabla \times \left(\frac{1}{\mu_b}\mathbf{f}_2 \right) = \mathbf{J}. \tag{13}$$

The derivation is detailed in section 4.2. With a particular choice of $\mathbf{f}_{3,k}, \mathbf{f}_{4,k}$ (given in subsection 4.4), we obtain the following formula:

$$\alpha_m = \frac{1}{i(\tilde{\omega}_m - \omega)} \int_{\Omega_{res}} \frac{(\varepsilon(\mathbf{r}, \tilde{\omega}_m) - \varepsilon_\infty(\mathbf{r}))}{(\varepsilon(\mathbf{r}, \omega) - \varepsilon_\infty(\mathbf{r}))}\mathbf{J}(\mathbf{r}) \cdot \mathbf{E}_m(\mathbf{r}) d\mathbf{r} \tag{14}$$

This formula can also be obtained by expanding an auxiliary field into its modal components and computing $\mathbf{E}_S$ from this auxiliary field. This process is detailed in subsection 4.4 and linked with alternative expressions of Green's kernel given in Muljarov and Langbein (2016) and another formula proposed by Wu et al. (2019).

The modal solution is given as

$$\mathbf{E}_S^{\text{modal}} = \sum_{m=1}^{N} \alpha_m \mathbf{E}_m \tag{15}$$

where N is the number of modes conserved. The formulas (8), (10), (9), (12) and (14) for coefficients α_m will provide a field $\mathbf{E}_S^{\text{modal}}$ that will converge to the scattered field $\mathbf{E}_S$ when N tends to the size of matrix $\mathbf{M}_h$. Their convergence rate, however, may differ.

3 Eigenmode expansion for first-order formulation of Maxwell's equations

In this section, we note $\mathbf{E}, \mathbf{H}$ the solutions of Maxwell's system (2). The permittivity $\varepsilon(\omega)$ is modeled by the relation (4) and the permeability $\mu = \mu_b$ is non-dispersive.

3.1 Discrete expansion

In order to linearize Maxwell's equations with respect to ω, auxiliary fields $\mathbf{P}_k$ (known as the polarization) and $\mathbf{Q}_k$ (known as the current) are introduced :

$$\mathbf{P}_k = \frac{c_k - i\omega\sigma_k}{\omega^2 - \omega_{0,k}^2 + i\gamma_k\omega}\mathbf{E}, \quad \mathbf{Q}_k = -i\omega\mathbf{P}_k$$

These auxiliary fields exist only inside the resonator. With elementary algebraic manipulations, we can reformulate Maxwell's system (2) as the following source problem

$$\left\{\begin{array}{lcl} -i\,\omega\,\varepsilon_\infty\,\mathbf{E} + \left(\sum_{k=1}^{L}\mathbf{Q}_k\right) - \nabla\times\mathbf{H} & = & \mathbf{J} \\ -i\,\omega\,\mu_b\,\mathbf{H} + \nabla\times\mathbf{E} & = & 0 \\ -i\omega\mathbf{P}_k - \mathbf{Q}_k & = & 0 \\ -i\omega\mathbf{Q}_k + \gamma_k\mathbf{Q}_k + \omega_{0,k}^2\mathbf{P}_k - c_k\mathbf{E} + i\omega\sigma_k\mathbf{E} & = & 0 \end{array}\right. \tag{16}$$

inside the resonator. Outside the resonator, we consider homogeneous Maxwell's equations

$$\left\{\begin{array}{lcl} -i\,\omega\,\varepsilon_b\mathbf{E} - \nabla\times\mathbf{H} & = & 0 \\ -i\,\omega\mu_b\mathbf{H} + \nabla\times\mathbf{E} & = & 0 \end{array}\right. \tag{17}$$

We can write this system using the linear operators $\mathbf{K}$ and $\mathbf{M}$

$$\mathbf{K}\mathbf{U} - i\omega\mathbf{M}\mathbf{U} = \mathbf{F}$$

with

$$\mathbf{K} = \begin{bmatrix} 0 & -\nabla\times & 0 & 1 \\ \nabla\times & 0 & 0 & 0 \\ 0 & 0 & 0 & -1 \\ -c_k & 0 & \omega_{0,k}^2 & \gamma_k \end{bmatrix}, \quad \mathbf{M} = \begin{bmatrix} \varepsilon_e & 0 & 0 & 0 \\ 0 & \mu_b & 0 & 0 \\ 0 & 0 & 1 & 0 \\ -\sigma_k & 0 & 0 & 1 \end{bmatrix}, \quad \mathbf{U} = \begin{bmatrix} \mathbf{E} \\ \mathbf{H} \\ \mathbf{P}_k \\ \mathbf{Q}_k \end{bmatrix}, \quad \mathbf{F} = \begin{bmatrix} \mathbf{J} \\ 0 \\ 0 \\ 0 \end{bmatrix},$$

where

$$\varepsilon_e = \left\{\begin{array}{l} \varepsilon_\infty \text{ in } \Omega_{res} \\ \varepsilon_b, \text{ elsewhere.} \end{array}\right.$$

The unknowns $\mathbf{P}_k$ and $\mathbf{Q}_k$ have degrees of freedom only inside the resonator. After discretization, the Maxwell's system is then given as

$$-i\omega\mathbf{M}_h\mathbf{U}_h + \mathbf{K}_h\mathbf{U}_h = \mathbf{F}_h \tag{18}$$

where $\mathbf{U}_h = (\mathbf{E}_h, \mathbf{H}_h, \mathbf{P}_h, \mathbf{Q}_h)$, and $\mathbf{E}_h, \mathbf{H}_h, \mathbf{P}_h, \mathbf{Q}_h$ contain the components of $\mathbf{E}, \mathbf{H}, \mathbf{P}_k, \mathbf{Q}_k$ on basis functions. The source term $\mathbf{F}_h$ is given as

$$(\mathbf{F}_h)_i = \int_{\Omega_{res}} \mathbf{J}(\mathbf{r}) \cdot \boldsymbol{\varphi}_i(\mathbf{r})\, d\mathbf{r}$$

where $\boldsymbol{\varphi}_i$ are basis functions for unknown $\mathbf{E}_h$. Matrices $\mathbf{M}_h$ and $\mathbf{K}_h$ and basis functions $\boldsymbol{\varphi}_i$ are given in appendix A.1. The right eigenvectors $\mathbf{x}_m$ solve the eigenproblem

$$\mathbf{K}_h\mathbf{x}_m = \lambda_m\mathbf{M}_h\mathbf{x}_m \tag{19}$$

where the eigenvalue λ_m is linked with $\tilde{\omega}_m$ by

$$\lambda_m = i\tilde{\omega}_m.$$

$\mathbf{x}_m^\perp$ is the left eigenvector of generalized eigenproblem (19) and solve the following eigenproblem

$$\mathbf{K}_h^T\mathbf{x}_m^\perp = \lambda_m\mathbf{M}_h^T\mathbf{x}_m^\perp \tag{20}$$

Remark 1. *The eigenvectors $\boldsymbol{x}_m^\perp$ and $\boldsymbol{x}_m$ can be chosen such that they satisfy the following biorthogonality relation*

$$\langle \boldsymbol{M}_h\boldsymbol{x}_m, \boldsymbol{x}_n^\perp\rangle = \delta_{m,n}$$

where $\delta_{m,n}$ is the Kronecker symbol.

Proof. Assuming that $\mathbf{M}_h^{-1}\mathbf{K}_h$ is diagonalizable, we have

$$\mathbf{M}_h^{-1}\mathbf{K}_h = \mathbf{V}\mathbf{D}\mathbf{V}^{-1}$$

where $\mathbf{D}$ is a diagonal matrix with eigenvalues λ_m on the diagonal and $\mathbf{V}$ the matrix whose columns are formed with right eigenvectors $\mathbf{x}_m$. The left eigenvectors of $\mathbf{M}_h^{-1}\mathbf{K}_h$ denoted $\mathbf{w}_m$ are the rows of matrix $\mathbf{V}^{-1}$. Since $\mathbf{V}\mathbf{V}^{-1} = \mathbf{I}$, vectors $\mathbf{x}_m$ and $\mathbf{w}_m$ are biorthogonal

$$\langle \mathbf{x}_m, \mathbf{w}_n\rangle = \delta_{m,n}$$

The left eigenvectors $\mathbf{w}_m$ can also be found by searching right eigenvectors of the transpose of $\mathbf{M}_h^{-1}\mathbf{K}_h$:

$$\mathbf{K}_h^T\mathbf{M}_h^{-T}\mathbf{w}_m = \lambda_m\mathbf{w}_m$$

By introducing $\mathbf{x}_m^\perp = \mathbf{M}_h^{-T}\mathbf{w}_m$, we obtain

$$\mathbf{K}_h^T\mathbf{x}_m^\perp = \lambda_m\mathbf{M}_h\mathbf{x}_m^\perp,$$

which corresponds to the eigenvalue problem (20). The biorthogonality relation is obtained directly by stating:

$$\langle \mathbf{x}_m, \mathbf{w}_n\rangle = \langle \mathbf{x}_m, \mathbf{M}_h^T\mathbf{x}_m^\perp\rangle = \langle \mathbf{M}_h\mathbf{x}_m, \mathbf{x}_m^\perp\rangle = \delta_{m,n}$$

□

The solution $\mathbf{U}_h$ is expanded with right eigenvectors $\mathbf{x}_m$ (they form a basis if the matrix $\mathbf{M}_h^{-1}\mathbf{K}_h$ is diagonalizable):

$$\mathbf{U}_h = \sum_m \alpha_m\mathbf{x}_m$$

By injecting this expansion in (18) and using (19)), we obtain

$$\sum_m \alpha_m(-i\,\omega + i\,\tilde{\omega}_m)\mathbf{M}_h\mathbf{x}_m = \mathbf{F}_h$$

The modal coefficient α_m is directly obtained by taking the scalar product $\langle,\rangle$ with the left eigenvector $\mathbf{x}_m^\perp$

$$\alpha_m(-i\,\omega + i\,\tilde{\omega}_m) = \langle \mathbf{F}_h, \mathbf{x}_m^\perp\rangle$$

As a result we obtain the relation

$$\alpha_m = \frac{1}{i(\tilde{\omega}_m - \omega)}\langle \mathbf{F}_h, \mathbf{x}_m^\perp\rangle \tag{21}$$

which is the announced result in the sub-section 2.2.

3.2 Link with continuous expansion

The left eigenvector $\mathbf{x}_m^\perp$ of the system (18) can be obtained directly from the right eigenvector $\mathbf{x}_m$ with the following theorem:

Theorem 1. *The left eigenvector* $\boldsymbol{x}_m^\perp = \left(\boldsymbol{E}_m^\perp, \boldsymbol{H}_m^\perp, \boldsymbol{P}_m^\perp, \boldsymbol{Q}_m^\perp\right)$ *of the eigenproblem* (19) *is given as*

$$\begin{cases} \boldsymbol{E}_m^\perp = \boldsymbol{E}_m \\ \boldsymbol{H}_m^\perp = -\boldsymbol{H}_m \\ \boldsymbol{P}_{m,k}^\perp = \dfrac{\omega_{0,k}^2}{c_k - \lambda_m \sigma_k} \boldsymbol{P}_{m,k} \\ \boldsymbol{Q}_{m,k}^\perp = -\dfrac{1}{c_k - \lambda_m \sigma_k} \boldsymbol{Q}_{m,k} \end{cases}$$

where $\boldsymbol{x}_m = (\boldsymbol{E}_m, \boldsymbol{H}_m, \boldsymbol{P}_m, \boldsymbol{Q}_m)$ *is the right eigenvector of* (19).

Proof. The proof is written at a continuous level without replacing the curl operator by the associated finite element matrix. The transposition of this proof at a discrete level is actually immediate since the last three equations (18) are expressed directly on quadrature points as detailed in appendix A. The left eigenvector $\mathbf{x}_m^\perp = \left(\mathbf{E}_m^\perp, \mathbf{H}_m^\perp, \mathbf{P}_m^\perp, \mathbf{Q}_m^\perp\right)$ solves the eigenproblem (20):

$$\begin{cases} \lambda_m \varepsilon_e \mathbf{E}_m^\perp - \lambda_m \left(\displaystyle\sum_{k=1}^{L} \sigma_k \mathbf{Q}_{m,k}^\perp \right) = \nabla \times \mathbf{H}_m^\perp - \left(\displaystyle\sum_{k=1}^{L} c_k \mathbf{Q}_{m,k}^\perp \right) \\ \lambda_m \mu_b \mathbf{H}_m^\perp = -\nabla \times \mathbf{E}_m^\perp \\ \lambda_m \mathbf{P}_{m,k}^\perp = \omega_{0,k}^2 \mathbf{Q}_{m,k}^\perp \\ \lambda_m \mathbf{Q}_{m,k}^\perp = \mathbf{E}_m^\perp - \mathbf{P}_{m,k}^\perp + \gamma_k \mathbf{Q}_{m,k}^\perp \end{cases} \tag{22}$$

We express $\mathbf{P}_{m,k}^\perp$ and $\mathbf{P}_{m,k}^\perp$ with only $\mathbf{E}_m^\perp$:

$$\mathbf{P}_{m,k}^\perp = \frac{\omega_{0,k}^2}{\lambda_m^2 + \omega_{0,k}^2 - \gamma_k \lambda_m} \mathbf{E}_m^\perp, \quad \mathbf{Q}_{m,k}^\perp = \frac{\lambda_m}{\lambda_m^2 + \omega_{0,k}^2 - \gamma_k \lambda_m} \mathbf{E}_m^\perp$$

The unknown $\mathbf{H}_m^\perp$ is also substituted to obtain a system in $\mathbf{E}_m$ only:

$$\lambda_m^2 \left(\varepsilon_e + \frac{c_k - \lambda_m \sigma_k}{\lambda_m^2 + \omega_{0,k}^2 - \gamma_k \lambda_m} \mathbf{1}_R \right) \mathbf{E}_m^\perp + \nabla \times \left(\frac{1}{\mu_b} \nabla \times \mathbf{E}_m^\perp \right) = 0$$

where $\mathbf{1}_R$ is the indicator function of Ω_{res}. This is the same eigenvalue problem solved by $\mathbf{E}_m$. Therefore, with an appropriate normalization, we can set $\mathbf{E}_m^\perp = \mathbf{E}_m$. By using the second equation of (22), we obtain $\mathbf{H}_m^\perp = -\mathbf{H}_m$. Since, we have

$$\mathbf{P}_{m,k} = \frac{c_k - \lambda_m \sigma_k}{\lambda_m^2 + \omega_{0,k}^2 - \gamma_k \lambda_m} \mathbf{E}_m, \quad \mathbf{Q}_{m,k} = -\lambda_m \mathbf{P}_{m,k}$$

we obtain

$$\mathbf{P}_{m,k}^\perp = \frac{\omega_{0,k}^2}{c_k - \lambda_m \sigma_k} \mathbf{P}_{m,k}, \quad \mathbf{Q}_{m,k}^\perp = -\frac{1}{c_k - \lambda_m \sigma_k} \mathbf{Q}_{m,k}.$$

□

The following theorem makes the link between the discrete formula (21) and the continuous formula (8):

Theorem 2. *The formula* (21) *is the discrete equivalent of* (8).

Proof. We use the fact that the source is non-null only for the equation in $\mathbf{E}$:

$$\langle \mathbf{F}_h, \mathbf{x}_m^\perp \rangle = \sum_i E_{m,i}^\perp \int_{\Omega_{res}} \mathbf{J}(\mathbf{r}) \cdot \boldsymbol{\varphi}_i(\mathbf{r}) dr$$

where $E_{m,i}^\perp$ is the i-th component of $\mathbf{E}_m^\perp$. By swapping the sum and the integral, we obtain

$$\langle \mathbf{F}_h, \mathbf{x}_m^\perp \rangle = \int_{\Omega_{res}} \mathbf{J}(\mathbf{r}) \cdot \mathbf{E}_m^\perp(\mathbf{r}) dr$$

Finally, we use that $\mathbf{E}_m^\perp = \mathbf{E}_m$ (theorem 1) to obtain

$$\langle \mathbf{F}_h, \mathbf{x}_m^\perp \rangle = \int_{\Omega_{res}} \mathbf{J}(\mathbf{r}) \cdot \mathbf{E}_m(\mathbf{r}) dr.$$

□

We have a similar theorem for the normalizations:

Theorem 3. *The normalization* (7) *with the left eigenvector given in theorem 1 is the discrete equivalent of* (11).

Proof. Similarly to the previous proof, we have the following equality

$$\begin{aligned}\langle \mathbf{M}_h \mathbf{x}_m, \mathbf{x}_m^\perp \rangle = & \int_\Omega \varepsilon_e \mathbf{E}_m \cdot \mathbf{E}_m^\perp + \mu_b \mathbf{H}_m \cdot \mathbf{H}_m^\perp \, d\Omega \\ & + \int_{\Omega_{res}} \left(\sum_{k=1}^{L} \mathbf{P}_{m,k} \cdot \mathbf{P}_{m,k}^\perp + (\mathbf{Q}_{m,k} - \sigma_k \mathbf{E}_{m,k}) \cdot \mathbf{Q}_m^\perp \right) d\Omega_{res}\end{aligned}$$

The left eigenvector is substituted by using theorem 1 and the relation $\lambda_m = i\tilde{\omega}_m$ to obtain

$$\begin{aligned}\langle \mathbf{M}_h \mathbf{x}_m, \mathbf{x}_m \rangle = & \int_\Omega \varepsilon_e \mathbf{E}_m \cdot \mathbf{E}_m - \mu_b \mathbf{H}_m \cdot \mathbf{H}_m \, d\Omega \\ & + \int_{\Omega_{res}} \left(\sum_{k=1}^{L} \frac{\omega_{0,k}^2}{c_k - i\tilde{\omega}_m \sigma_k} \mathbf{P}_{m,k} \cdot \mathbf{P}_{m,k} - \frac{1}{c_k - i\tilde{\omega}_m \sigma_k} (\mathbf{Q}_{m,k} - \sigma_k \mathbf{E}_{m,k}) \cdot \mathbf{Q}_m \right) d\Omega_{res}\end{aligned}$$

$\mathbf{P}_m$ and $\mathbf{Q}_m$ are replaced to obtain

$$\begin{aligned}\langle \mathbf{M}_h \mathbf{x}_m, \mathbf{x}_m \rangle = & \int_\Omega \varepsilon_e \mathbf{E}_m \cdot \mathbf{E}_m - \mu_b \mathbf{H}_m \cdot \mathbf{H}_m \, d\Omega \\ & + \int_{\Omega_{res}} \left(\sum_{k=1}^{L} \frac{(\omega_{0,k}^2 + \tilde{\omega}_m^2) c_k + i\sigma_k \tilde{\omega}_m (-2\omega_{0,k}^2 + i\gamma_k \tilde{\omega}_m)}{(-\tilde{\omega}_m^2 + \omega_{0,k}^2 - i\gamma_k \tilde{\omega}_m)^2} \mathbf{E}_m \cdot \mathbf{E}_m \right) d\Omega_{res}\end{aligned}$$

A simple computation of the derivative of $\omega\varepsilon(\omega)$ with respect to ω provide the same expressions. As a result, we have proven that

$$\langle \mathbf{M}_h \mathbf{x}_m, \mathbf{x}_m \rangle = \int_\Omega \frac{\partial \left(\tilde{\omega}_m \varepsilon(\tilde{\omega}_m) \right)}{\partial \tilde{\omega}_m} \mathbf{E}_m \cdot \mathbf{E}_m - \mu_b \mathbf{H}_m \; cdot \mathbf{H}_m \, d\Omega.$$

This relation proves that the normalization (7) is the discrete equivalent of (11). □

Remark 2. *The normalization can be written with only unknown $\boldsymbol{E}_m$:*

$$\langle \boldsymbol{M}_h \boldsymbol{x}_m, \boldsymbol{x}_m \rangle = \int_\Omega \frac{\partial\left(\tilde{\omega}_m \varepsilon(\tilde{\omega}_m)\right)}{\partial \tilde{\omega}_m} \boldsymbol{E}_m \cdot \boldsymbol{E}_m + \varepsilon(\tilde{\omega}_m) \boldsymbol{E}_m \cdot \boldsymbol{E}_m d\Omega.$$

The result is obtained directly by using the relation $\boldsymbol{H}_m = \dfrac{1}{i\omega\mu_b}\nabla \times \boldsymbol{E}_m$ and the variational formulation satisfied by $\boldsymbol{E}_m$ (with only Dirichlet or Neumann boundary conditions):

$$-\tilde{\omega}_m^2 \int_\Omega \varepsilon(\tilde{\omega}_m) \boldsymbol{E}_m \cdot \boldsymbol{E}_m \, d\Omega + \int_\Omega \frac{1}{\mu_b} \nabla \times \boldsymbol{E}_m \cdot \nabla \times \boldsymbol{E}_m \, d\Omega = 0.$$

4 Derivation of other formulas and issues

4.1 Derivation with an alternative source

To obtain the formula (8), first, we have written Maxwell's equations directly for the scattered field $\mathbf{E}_S(\mathbf{r},\omega), \mathbf{H}_S(\mathbf{r},\omega)$ and then introduced the auxiliary fields $\mathbf{P}$ and $\mathbf{Q}$. In the aforementioned paper Yan et al. (2018), Maxwell's equations are first written for the total field, and the auxiliary unknowns $\mathbf{P}$ and $\mathbf{Q}$ are introduced at this step. Hence the unknowns $\mathbf{E}, \mathbf{H}, \mathbf{P}, \mathbf{Q}$ solve the system (16) with $\mathbf{J} = 0$. As a second step, we subtract the equations solved by the incident field (homogeneous Maxwell's equation with indices ε_b and μ_b), and use the relations

$$[\mathbf{E}(\mathbf{r},\omega), \mathbf{H}(\mathbf{r},\omega)] = \left[\mathbf{E}_S(\mathbf{r},\omega) + \mathbf{E}_{\text{inc}}(\mathbf{r},\omega),\ \mathbf{H}_S(\mathbf{r},\omega) + \mathbf{H}_{\text{inc}}(\mathbf{r},\omega)\right]$$

to obtain the system solved by $(\mathbf{E}_S, \mathbf{H}_S, \mathbf{P}_{T,k}, \mathbf{Q}_{T,k})$ inside the resonator:

$$\begin{cases} -i\,\omega\,\varepsilon_\infty\,\mathbf{E}_S + \left(\displaystyle\sum_{k=1}^{L} \mathbf{Q}_{T,k}\right) - \nabla \times \mathbf{H}_S & = & i\omega(\varepsilon_\infty - \varepsilon_b)\mathbf{E}_{\text{inc}} \\ -i\,\omega\,\mu_b\,\mathbf{H}_S + \nabla \times \mathbf{E}_S & = & 0 \\ -i\omega\mathbf{P}_{T,k} - \mathbf{Q}_{T,k} & = & 0 \\ -i\omega\mathbf{Q}_{T,k} + \gamma_k\mathbf{Q}_{T,k} + \omega_0^2\mathbf{P}_{T,k} - (c_k - i\omega\sigma_k)\mathbf{E}_S & = & (c_k - i\omega\sigma_k)\mathbf{E}_{\text{inc}} \end{cases} \tag{23}$$

The auxiliary fields $\mathbf{P}_{T,k}, \mathbf{Q}_{T,k}$ here represent the total polarization and current whereas in the previous section we had introduced the scattered polarization $\mathbf{P}_k$ and current $\mathbf{Q}_k$. Unlike the equations considered in section 3, we can see that the source term on the right hand side of the equations is no longer confined to the first equation. The coefficient α_m becomes (by using formula (6) and biorthogonal vectors given in theorem (1)):

$$\alpha_m = \frac{1}{i(\tilde{\omega}_m - \omega)} \left[\int_{\Omega_{res}} i\omega(\varepsilon_\infty - \varepsilon_b)\mathbf{E}_m \cdot \mathbf{E}_{\text{inc}} + \frac{(c_k - i\omega\sigma_k) i\tilde{\omega}_m}{(-\tilde{\omega}_m^2 + \omega_{0,k}^2 - i\gamma\tilde{\omega}_m)} \mathbf{E}_m \cdot \mathbf{E}_{\text{inc}} d\Omega_{res} \right]$$

that can be written as

$$\alpha_m = \int_{\Omega_{res}} (\varepsilon_b - \varepsilon_\infty)\mathbf{E}_{\text{inc}} \cdot \mathbf{E}_m d\Omega + \frac{\tilde{\omega}_m}{\tilde{\omega}_m - \omega} \int_{\Omega_{res}} (\varepsilon(\tilde{\omega}_m) - \varepsilon_b)\mathbf{E}_{\text{inc}} \cdot \mathbf{E}_m d\Omega,$$

which is the announced formula (9). It is important to notice that the systems (23) and (16) provide exactly the same numerical solution $\mathbf{E}_S$ (and also the same $\mathbf{H}_S$). Only the auxiliary

fields $\mathbf{P}$ and $\mathbf{Q}$ differ, that's why the source $\mathbf{F}_h$ is different between the two approaches and two different formulas are obtained for α_m. Other formulas for α_m can be found by choosing a different distribution of the source over the four equations. This is the object of the next sub-section.

Remark 3. *The formula* (9) *has been obtained through discretized Maxwell's equations and with biorthogonal projection. It has also been derived in a different way by using the divergence theorem and the continuous operator, not the discretized one, in (Yan et al., 2018).*

4.2 Generalized Sources

Let us split the source term $\mathbf{J}$ into a set of artificial sources denoted $\mathbf{f}_1, \mathbf{f}_2, \mathbf{f}_{3,k}, \mathbf{f}_{4,k}$ inside the resonator.

$$\left\{\begin{array}{lcl} -i\,\omega\,\varepsilon_\infty\,\mathbf{E} + \left(\sum_{k=1}^{L}\mathbf{Q}_k\right) - \nabla\times\mathbf{H} & = & \mathbf{f}_1 \\ -i\,\omega\,\mu_b\,\mathbf{H} + \nabla\times\mathbf{E} & = & \mathbf{f}_2 \\ -i\omega\mathbf{P}_k - \mathbf{Q}_k & = & \mathbf{f}_{3,k} \\ -i\omega\mathbf{Q}_k + \gamma_k\mathbf{Q}_k + \omega_{0,k}^2\mathbf{P}_k - (c_k - i\omega\sigma_k)\mathbf{E} & = & \mathbf{f}_{4,k} \end{array}\right. \tag{24}$$

By abuse of notation, we kept the same names for auxiliary fields $\mathbf{H}, \mathbf{P}_k, \mathbf{Q}_k$, but these auxiliary fields are different from the fields introduced in section 3, only the field $\mathbf{E}$ will be the same. We can now obtain an infinity of formulas for α_m:

Theorem 4. *There exists an infinity of formulas for α_m, e.g.*

$$\alpha_m = \frac{1}{i(\omega-\tilde{\omega}_m)}\int_{\Omega_{res}} \boldsymbol{f}_1\cdot\boldsymbol{E}_m - \boldsymbol{f}_2\cdot\boldsymbol{H}_m + \left(\sum_{k=1}^{L}\frac{\left(\omega_{0,k}^2\boldsymbol{f}_{3,k} + i\tilde{\omega}_m\boldsymbol{f}_{4,k}\right)}{-\tilde{\omega}_m^2+\omega_{0,k}^2 - i\gamma_k\tilde{\omega}_m}\cdot\boldsymbol{E}_m\right) d\Omega_{res}$$

as soon as

$$\int_{\Omega_{res}}\left(\boldsymbol{f}_1 + \sum_{k=1}^{L}\frac{i\omega\boldsymbol{f}_{4,k}+\omega_{0,k}^2\boldsymbol{f}_{3,k}}{-\omega^2 - i\omega\gamma_k + \omega_{0,k}^2}\right)\cdot\boldsymbol{\varphi}_i + \frac{i}{\omega\mu_b}\boldsymbol{f}_2\cdot\nabla\times\boldsymbol{\varphi}_i\, d\Omega_{res} = \int_{\Omega_{res}}\boldsymbol{J}\cdot\boldsymbol{\varphi}_i d\Omega_{res} \tag{25}$$

for all test-functions $\boldsymbol{\varphi}_i$. If the function $\boldsymbol{f}_2$ is chosen continuous in Ω, we obtain the condition (13).

Proof. The fourth equation of (24) is multiplied by $-i\omega$ and P is substituted to obtain:

$$\mathbf{Q}_k = \frac{-i\omega\mathbf{f}_{4,k} - \omega_{0,k}^2\mathbf{f}_{3,k}}{-\omega^2 - i\omega\gamma_k + \omega_{0,k}^2} - i\omega\frac{(c_k - i\omega\sigma_k)}{-\omega^2 - i\omega\gamma_k + \omega_{0,k}^2}\mathbf{E}$$

The second equation of (24) provides

$$-i\omega\mathbf{H} = \frac{\mathbf{f}_2}{\mu_b} - \frac{1}{\mu_b}\nabla\times\mathbf{E}$$

We inject these expressions of $\mathbf{H}$ and $\mathbf{Q}_k$ in the variational formulation of the first equation of (24) to obtain the variational formulation satisfied by $\mathbf{E}$:

$$-\omega^2\int_\Omega \varepsilon(\omega)\mathbf{E}\cdot\boldsymbol{\varphi}_i + \frac{1}{\mu_b}(\nabla\times\mathbf{E})\cdot(\nabla\times\boldsymbol{\varphi}_i)\, d\Omega = -i\omega\int_\Omega\left[\mathbf{f}_1 + \frac{\left(i\omega\mathbf{f}_{4,k}+\omega_{0,k}^2\mathbf{f}_{3,k}\right)}{-\omega^2 - i\omega\gamma_k + \omega_{0,k}^2} + \frac{i}{\omega\mu_b}\mathbf{f}_2\cdot\nabla\times\boldsymbol{\varphi}_i\right] d\Omega$$

By equalling the right-hand side with $-i\omega \int_\Omega \mathbf{J} \cdot \boldsymbol{\varphi}_i d\Omega$, we obtain the condition (25). This condition implies the continuous condition (13) if $\mathbf{f}_2$ is continuous in Ω. The formula for α_m is given by

$$\alpha_m = \frac{1}{i(\omega - \tilde{\omega}_m)} \int_\Omega \mathbf{f}_1 \cdot \mathbf{E}_m^\perp + \mathbf{f}_2 \cdot \mathbf{H}_m^\perp + \left(\sum_{k=1}^{L} \mathbf{f}_{3,k} \cdot \mathbf{P}_{m,k}^\perp + \mathbf{f}_{4,k} \cdot \mathbf{Q}_{m,k}^\perp \right) d\Omega.$$

By using theorem (1), we obtain the claimed expression for α_m. □

By choosing different splittings of the source (i.e. different functions $\mathbf{f}_1, \mathbf{f}_2, \mathbf{f}_3, \mathbf{f}_4$ that satisfy the relationship above), we will obtain different formulas for α_m. The modal solution obtained with these different formulas (see equation (15)) will converge towards the same electric field $\mathbf{E}_S$ when the number of modes is increased.

4.3 Derivation with second-order formulation of Maxwell's equations

In this section we propose a different linearization of the problem by starting from the second order formulation. With this alternative linearization, we obtain the formula (10) for the coefficients α_m. Let us start from the second-order formulation of Maxwell's equations

$$-\omega^2 \varepsilon(\omega)\mathbf{E} + \nabla \times \left(\frac{1}{\mu_b} \nabla \times \mathbf{E} \right) = -i\omega \mathbf{J}.$$

In order to linearize this equation, let us introduce the field $\mathbf{E}' = -i\omega\mathbf{E}$ and the auxiliary field $\mathbf{P}' = (\varepsilon(\omega) - \varepsilon_\infty)\,\mathbf{E}'$ and $\mathbf{Q}' = -i\omega\mathbf{P}'$. We obtain the following system of linear equations:

$$\left\{ \begin{array}{lcl} -i\,\omega\mathbf{E} - \mathbf{E}' & = & 0 \\ -i\,\omega\varepsilon_\infty \mathbf{E}' + \left(\sum_{k=1}^{L} \mathbf{Q}_k' \right) + \nabla \times \left(\frac{1}{\mu_b} \nabla \times \mathbf{E} \right) & = & -i\,\omega\mathbf{J} \\ -i\,\omega\mathbf{P}_k' - \mathbf{Q}_k' & = & 0 \\ -i\omega\mathbf{Q}_k' + \gamma_k \mathbf{Q}_k' + \omega_{0,k}^2 \mathbf{P}_k' - (c_k - i\omega\sigma_k)\mathbf{E}' & = & 0 \end{array} \right. , \tag{26}$$

inside the resonator which gives the following stiffness and mass operators $\mathbf{K}$ and $\mathbf{M}$ for the vector $\mathbf{U} = [\mathbf{E}, \mathbf{E}', \mathbf{P}', \mathbf{Q}']$:

$$\mathbf{K} = \begin{bmatrix} 0 & -1 & 0 & 0 \\ \frac{1}{\mu_b} \nabla \times \nabla \times & 0 & 0 & 1 \\ 0 & 0 & 0 & -1 \\ 0 & -c_k & \omega_{0,k}^2 & \gamma_k \end{bmatrix},$$

$$\mathbf{M} = \begin{bmatrix} 1 & 0 & 0 & 0 \\ 0 & \varepsilon_e & 0 & 0 \\ 0 & 0 & 1 & 0 \\ 0 & -\sigma_k & 0 & 1 \end{bmatrix}.$$

As a result, Maxwell's equations are rewritten as :

$$(-i\,\omega\mathbf{M} + \mathbf{K})\mathbf{U} = \mathbf{F},$$

where

$$\mathbf{F} = [0, -i\omega\mathbf{J}, 0, 0]$$

is the source term. After discretization, we have the following discrete system

$$(-i\omega\mathbf{M}_h + \mathbf{K}_h)\mathbf{U}_h = \mathbf{F}_h.$$

The matrices $\mathbf{M}_h, \mathbf{K}_h$ are given in appendix A.2. For sake of simplicity, the following developments will be made with the continuous operators $\mathbf{K}$ and $\mathbf{M}$, but the extension to the discrete operators $\mathbf{M}_h$ and $\mathbf{K}_h$ is straightforward. We obtain the following system of equations for the biorthogonal eigenvectors ($\mathbf{x}_m^\perp = [\mathbf{E}_\perp, \mathbf{E}'_\perp, \mathbf{P}'_\perp, \mathbf{Q}'_\perp]$):

$$\left\{\begin{array}{lcl} -i\,\tilde{\omega}_m\mathbf{E}_\perp + \nabla\times\left(\dfrac{1}{\mu_b}\nabla\times\mathbf{E}'_\perp\right) & = & 0 \\ -i\,\tilde{\omega}_m\varepsilon_\infty\mathbf{E}'_\perp - \mathbf{E}_\perp - \left(\sum_{k=1}^{L}(c_k - i\tilde{\omega}_m\sigma_k)\mathbf{Q}'_{\perp,k}\right) & = & 0 \\ -i\,\tilde{\omega}_m\mathbf{P}'_{\perp,k} + \omega_{0,k}^2\mathbf{Q}'_{\perp,k} & = & 0 \\ -i\,\tilde{\omega}_m\mathbf{Q}'_{\perp,k} + \gamma_k\mathbf{Q}'_{\perp,k} + \mathbf{E}'_{\perp,k} - \mathbf{P}'_{\perp,k} & = & 0, \end{array}\right.$$

By eliminating the other variables, we can show that $\mathbf{E}'_\perp$ verifies

$$-\tilde{\omega}_m^2\varepsilon(\tilde{\omega}_m)\mathbf{E}'_\perp + \nabla\times\left(\frac{1}{\mu_0}\nabla\times\mathbf{E}'_\perp\right) = 0,$$

and subsequentially :

$$\left\{\begin{array}{lcl} \mathbf{E}'_\perp & = & \mathbf{E}_m \\ \mathbf{E}_\perp & = & -i\tilde{\omega}_m\varepsilon(\tilde{\omega}_m)\mathbf{E}_m \\ \mathbf{P}'_{\perp,k} & = & \dfrac{\omega_{0,k}^2}{\omega_{0,k}^2 - i\gamma_k\tilde{\omega}_m - \tilde{\omega}_m^2}\mathbf{E}_m \\ \mathbf{Q}'_{\perp,k} & = & \dfrac{i\,\tilde{\omega}_m}{\omega_{0,k}^2 - i\gamma_k\tilde{\omega}_m - \tilde{\omega}_m^2}\mathbf{E}_m, \end{array}\right.$$

where $\mathbf{E}_m$ is the E-component of the the left eigenvector $\mathbf{x}_m$. We can now obtain the excitation coefficient :

$$\alpha_m = \frac{1}{i\,(\tilde{\omega}_m - \omega)}\frac{\langle\mathbf{F}_h, \mathbf{x}_m^\perp\rangle}{\langle\mathbf{M}_h\mathbf{x}_m, \mathbf{x}_m^\perp\rangle} = \frac{-i\omega\displaystyle\int_{\Omega_{res}}\mathbf{J}(\mathbf{r})\cdot\mathbf{E}_m(r)d\mathbf{r}}{i(\tilde{\omega}_m - \omega)\,N_m},$$

where the coefficient N_m appears since we choose the normalization (11) of the first order formulation. N_m is given as

$$N_m = \langle\mathbf{M}_h\mathbf{x}_m, \mathbf{x}_m^\perp\rangle = \int_\Omega \mathbf{E}_m\cdot\mathbf{E}_\perp + \varepsilon_\infty\mathbf{E}'_m\cdot\mathbf{E}'_\perp d\Omega + \int_{\Omega_{res}}\left(\sum_{k=1}^{L}\mathbf{P}'_{m,k}\cdot\mathbf{P}'_{\perp,k} + \left(\mathbf{Q}'_{m,k} - \sigma_k\mathbf{E}'_m\right)\cdot\mathbf{Q}'_{\perp,k}\right)d\Omega_{res}.$$

By substituting $\mathbf{E}'_m, \mathbf{P}'_k, \mathbf{Q}'_k, \mathbf{E}_\perp, \mathbf{E}'_\perp, \mathbf{P}'_\perp, \mathbf{Q}'_\perp$ by their expression, we obtain

$$\begin{aligned} N_m = -i\tilde{\omega}_m\Big[& \int_\Omega \varepsilon(\tilde{\omega}_m)\mathbf{E}_m\cdot\mathbf{E}_m + \varepsilon_e\mathbf{E}_m\cdot\mathbf{E}_m d\Omega \\ & + \int_{\Omega_{res}}\frac{c_k(\omega_{0,k}^2 + \tilde{\omega}_m^2) + i\sigma_k\tilde{\omega}_m(i\gamma_k\tilde{\omega}_m - 2\omega_{0,k}^2)}{(\omega_0^2 - i\gamma_k\tilde{\omega}_m - \tilde{\omega}_m^2)^2}\mathbf{E}_m\cdot\mathbf{E}_m\,d\Omega_{res}\Big]. \end{aligned}$$

We recognize the normalization used by the first order formulation multiplied by $-i\tilde{\omega}_m$. As a result, if $\mathbf{E}_m$ is normalized by (11), we obtain that

$$N_m = -i\tilde{\omega}_m,$$

which gives us this expression for the excitation coefficient:

$$\alpha_m = \frac{\omega}{i\tilde{\omega}_m(\tilde{\omega}_m - \omega)} \int_{\Omega_{res}} \mathbf{J} \cdot \mathbf{E}_m d\Omega.$$

We recognize the formula (10).

4.4 Obtention of other formulas by using auxiliary fields

With the introduced linearization of section 3, the polarization field $\mathbf{P} = \sum_k \mathbf{P}_k$ can be reconstructed inside the resonator with the modal expansion:

$$\mathbf{P}_{\text{modal}} = \sum_{m=1}^{N} \alpha_m \mathbf{P}_m = \sum_{m=1}^{N} \alpha_m (\varepsilon(\tilde{\omega}_m) - \varepsilon_\infty)\mathbf{E}_m$$

and the scattered field $\mathbf{E}_S$ computed from $\mathbf{P}_{\text{modal}}$:

$$\mathbf{E}_S \approx \frac{\mathbf{P}_{\text{modal}}}{(\varepsilon(\omega) - \varepsilon_\infty)} = \sum_{m=1}^{N} \alpha_m \frac{(\varepsilon(\tilde{\omega}_m) - \varepsilon_\infty)}{(\varepsilon(\omega) - \varepsilon_\infty)} \mathbf{E}_m \tag{27}$$

At least this modal expansion will converge inside the resonator towards the scattered field $\mathbf{E}_S$ when the number of modes N increases. We can reinterpret the equation (27) as a new formula for α_m:

$$\alpha_m = \frac{1}{i(\tilde{\omega}_m - \omega)} \int_{\Omega_{res}} \frac{(\varepsilon(\mathbf{r}, \tilde{\omega}_m) - \varepsilon_\infty(\mathbf{r}))}{(\varepsilon(\mathbf{r}, \omega) - \varepsilon_\infty(\mathbf{r}))} \mathbf{J}(\mathbf{r}) \cdot \mathbf{E}_m(\mathbf{r}) d\mathbf{r}$$

which is the formula (14) announced in section 2.2. We can also choose the auxiliary field $\mathbf{Q} = \sum_k \mathbf{Q}_k$ and obtain the following formula

$$\alpha_m = \frac{1}{i(\tilde{\omega}_m - \omega)} \int_{\Omega_{res}} \frac{\tilde{\omega}_m(\varepsilon(\mathbf{r}, \tilde{\omega}_m) - \varepsilon_\infty(\mathbf{r}))}{\omega(\varepsilon(\mathbf{r}, \omega) - \varepsilon_\infty(\mathbf{r}))} \mathbf{J}(\mathbf{r}) \cdot \mathbf{E}_m(\mathbf{r}) d\mathbf{r} \tag{28}$$

It turns out that the two formulas (14) and (28) are also valid outside the resonator. For the formula (14), it can be proven by choosing appropriately the sources $\mathbf{f}_{3,k}, \mathbf{f}_{4,k}$:

Theorem 5. *The formula* (14) *provides a modal expansion valid outside the resonator.*

Proof. We choose

$$\mathbf{f}_1 = \mathbf{f}_2 = 0, \quad \mathbf{f}_{3,k} = \frac{c_k}{\omega_{0,k}^2} \frac{\mathbf{J}}{\varepsilon(\omega) - \varepsilon_\infty}, \quad \mathbf{f}_{4,k} = -\sigma_k \frac{\mathbf{J}}{\varepsilon(\omega) - \varepsilon_\infty}$$

in the system (24). We have

$$\sum_{k=1}^{L} \frac{i\omega \mathbf{f}_{4,k} + \omega_{0,k}^2 \mathbf{f}_{3,k}}{-\omega^2 - i\omega\gamma_k + \omega_{0,k}^2} = \left(\sum_{k=1}^{L} \frac{c_k - i\omega\sigma_k}{-\omega^2 - i\omega\gamma_k + \omega_{0,k}^2} \right) \frac{\mathbf{J}}{\varepsilon(\omega) - \varepsilon_\infty} = \mathbf{J}$$

As a result the condition (25) is satisfied and we can apply the theorem 4 to obtain a valid formula for α_m in all the computational domain:

$$\alpha_m = \frac{1}{i(\omega - \tilde{\omega}_m)} \int_{\Omega_{res}} \left(\sum_{k=1}^{L} \frac{\left(\omega_{0,k}^2 \mathbf{f}_{3,k} + i\tilde{\omega}_m \mathbf{f}_{4,k}\right)}{-\tilde{\omega}_m^2 + \omega_{0,k}^2 - i\gamma_k \tilde{\omega}_m} \cdot \mathbf{E}_m \right) d\Omega_{res}$$

which gives

$$\alpha_m = \frac{1}{i(\omega - \tilde{\omega}_m)} \int_{\Omega_{res}} \left(\sum_{k=1}^{L} \frac{c_k - i\tilde{\omega}_m \sigma_k}{-\tilde{\omega}_m^2 + \omega_{0,k}^2 - i\gamma_k \tilde{\omega}_m} \right) \frac{\mathbf{J} \cdot \mathbf{E}_m}{\varepsilon(\omega) - \varepsilon_\infty} d\Omega_{res}$$

The formula (14) is obtained. □

Remark 4. *The ratio* $\dfrac{(\varepsilon(\boldsymbol{r}, \tilde{\omega}_m) - \varepsilon_\infty(\boldsymbol{r}))}{(\varepsilon(\boldsymbol{r}, \omega) - \varepsilon_\infty(\boldsymbol{r}))}$ *in formula* (14) *is located inside the integral in order to handle correctly the case of several resonators with different coefficients* $\varepsilon_\infty, c_k, \gamma_k, \sigma_k, \omega_{0,k}$.

4.4.1 Case of an alternative source

In Wu et al. (2019), this process is applied with the alternative source of subsection 4.1. As a result, the following formula is obtained for the scattered field $\mathbf{E}_S$:

$$\mathbf{E}^S \approx -\mathbf{E}_{\text{inc}} + \sum_{m=1}^{N} \alpha_m^W \frac{(\varepsilon_{res}(\tilde{\omega}_m) - \varepsilon_\infty)}{(\varepsilon_{res}(\omega) - \varepsilon_\infty)} \tag{29}$$

where α_m^W is given by the equation (9):

$$\alpha_m^W = \int_{\Omega_{res}} (\varepsilon_b - \varepsilon_\infty) \mathbf{E}_{inc} \cdot \mathbf{E}_m d\Omega + \frac{\tilde{\omega}_m}{\tilde{\omega}_m - \omega} \int_{\Omega_{res}} (\varepsilon(\tilde{\omega}_m) - \varepsilon_b) \mathbf{E}_{inc} \cdot \mathbf{E}_m d\Omega$$

and $\varepsilon_{res}(\omega)$ is the permittivity inside the resonator. The formula (29) is valid only inside the resonator and cannot be reinterpreted as a new formula for α_m because of the presence of $-\mathbf{E}_{\text{inc}}$.

For a metallic material (e.g. $D > 0, \gamma_0 = 0$), the vector $(0, 0, P, 0)$ is a static eigenvector of (19) and is excited with the right hand side chosen in (23). As a result, the formula (29) will not be used for metallic materials. We have observed numerically that it did not converge to the correct solution in this case.

4.4.2 Link with formulas with poles of permittivity

In Muljarov and Langbein (2016) (formula A9 of appendix A), the following alternative formula is proposed

$$\alpha_m = \frac{1}{i(\tilde{\omega}_m - \omega)} \int_{\Omega_{res}} \frac{(\omega - \Omega_k)}{(\tilde{\omega}_m - \Omega_k)} \mathbf{J}(\mathbf{r}) \cdot \mathbf{E}_m(\mathbf{r}) d\mathbf{r} \tag{30}$$

where Ω_k is a pole of the refractive permittivity $\varepsilon(\omega)$. This formula is proved at a continuous level, but we have also observed that it remains valid at a discrete level for any pole of $\varepsilon(\omega)$:

Theorem 6. *The formula* (30) *provides a modal expansion valid outside the resonator.*

Proof. The proof is similar to the proof of theorem 5. It starts from the following linearization (we consider the model (3) with $D = 0$) of Maxwell's equations

$$\begin{cases} -i\omega\varepsilon_\infty \mathbf{E} - \left(\sum_k \widetilde{\mathbf{P}}_k\right) - \nabla \times \mathbf{H} = 0 \\ -i\omega\mu_b \mathbf{H} + \nabla \times \mathbf{E} = 0 \\ -i\omega\widetilde{\mathbf{P}}_k + i\Omega_k\widetilde{\mathbf{P}}_k + i\omega\sigma_k \mathbf{E} = \mathbf{f}_{3,k} \\ -i\omega\widetilde{\mathbf{Q}}_k - i\bar{\Omega}_k\widetilde{\mathbf{Q}}_k + i\omega\bar{\sigma}_k \mathbf{E} = 0 \end{cases} \tag{31}$$

This system has the same solution $\mathbf{E}$ as the system (16) by choosing

$$\mathbf{f}_{3,k} = (-i\omega + i\Omega_k)\mathbf{J}$$

The left eigenvector associated with the system (31) is given as

$$\widetilde{\mathbf{P}}^{\perp}_{m,k} = \frac{\mathbf{E}_m}{-i\tilde{\omega}_m + i\Omega_k}$$

As a result, we obtain the following formula for α_m

$$\alpha_m = \frac{1}{i(\tilde{\omega}_m - \omega)} \int_{\Omega_{res}} \mathbf{f}_{3,k} \cdot \widetilde{\mathbf{P}}^{\perp}_{m,k} d\Omega_{res} = \frac{1}{i(\tilde{\omega}_m - \omega)} \int_{\Omega_{res}} \frac{(-\omega + \Omega_k)}{(-\tilde{\omega}_m + \Omega_k)} \mathbf{J} \cdot \mathbf{E}_m d\Omega_{res}$$

which is the formula (30). As a result this formula provides a valid modal expansion in all the computational domain. □

The formula (14) can be seen as a combination of formulas (30) since all the poles of $\varepsilon(\omega)$ will be involved.

4.5 Treatment of degenerate eigenvalues

A set of degenerate modes $\{\mathbf{x}_k\}_{m_1 \leq k \leq m_2}$, are solutions of the eigenvalue problem at the same eigenfrequency $\tilde{\omega}_{m_1}$. Degenerate eigenvectors do not necessarily form an orthogonal sub-basis with respects to $\mathbf{M}_h$. However, using Gram-Schmidt orthogonalization process, an orthogonal sub-basis with respects to $\mathbf{M}_h$ can be constructed from the set of degenerate modes by algorithm 1. By applying this procedure, the formula (6) holds for degenerate eigenvalues with normaliza-

Algorithm 1 Algorithm to apply Gram-Schmidt orthogonalization to vectors $\mathbf{x}_m$

for m=m_1 to m_2 **do**
  Initialize $\mathbf{y} = \mathbf{x}_m$
  for j = m_1 to $m - 1$ **do**
    Compute $\alpha = \langle \mathbf{M}_h \mathbf{x}_m, \mathbf{x}_j^{\perp} \rangle$
    Substitute $\mathbf{y}$ by $\mathbf{y} - \alpha \mathbf{x}_j$
  end for
  Compute left eigenvector $\mathbf{y}^{\perp}$ from right eigenvector $\mathbf{y}$ by using theorem 1
  Substitute $\mathbf{x}_m$ by $\mathbf{y}/\langle \mathbf{M}_h \mathbf{y}, \mathbf{y}^{\perp} \rangle$
  Store $\mathbf{x}_j^{\perp} = \mathbf{y}^{\perp}/\langle \mathbf{M}_h \mathbf{y}, \mathbf{y}^{\perp} \rangle$
end for

tion (7). This process can also be done with continuous eigenmodes by replacing $\langle \mathbf{M}_h \mathbf{x}_m, \mathbf{x}_j^\perp \rangle$ by

$$\int_\Omega \frac{\partial(\tilde{\omega}_m \, \varepsilon(\tilde{\omega}_m))}{\partial \tilde{\omega}_m} \mathbf{E}_m \cdot \mathbf{E}_j - \frac{\partial \left(\tilde{\omega}_m \mu(\tilde{\omega}_m)\right)}{\partial \tilde{\omega_m}} \mathbf{H}_m \cdot \mathbf{H}_j d\Omega.$$

Here μ depends on ω inside the PML layers, which are detailed in the next sub-section. For elements inside the PML, the right eigenvector will be computed with formula (33) instead of theorem 1. In practice, we have observed degenerate eigenvalues due to PML layers or accumulation points. Accumulation points occur for poles and zeros of the permittivity $\varepsilon(\omega)$. In the 2-D transverse electric case (i.e. $\mathbf{E} = u\mathbf{e}_z$), we did not observe accumulation points for zeros of $\varepsilon(\omega)$.

4.6 PML

In this section, we describe how dispersive PMLs are handled. The damping coefficients σ_x, σ_y and σ_z inside a PML where $x > x_0$, $y > y_0$ or $z > z_0$ are parabolic:

$$\sigma_1 = \sigma_x = \frac{3\log(1000)}{2a^3}(x - x_0)^2 v_{max}\, \sigma$$

$$\sigma_2 = \sigma_y = \frac{3\log(1000)}{2a^3}(y - y_0)^2 v_{max}\, \sigma$$

$$\sigma_3 = \sigma_z = \frac{3\log(1000)}{2a^3}(z - z_0)^2 v_{max}\, \sigma.$$

The coefficient σ serves to adjust the reflection coefficient of the PML. v_{max} is the speed of the wave inside the PML and a is the thickness of PML layer. In this section, we describe the formulation used for dispersive PMLs. The matrices $\mathbf{M}_h, \mathbf{K}_h$ are no longer symmetric. We provide relations between the left eigenvector $\mathbf{x}_m^\perp$ and right eigenvector $\mathbf{x}_m$. As a result we do not need to compute the eigenvectors of the adjoint problem, since we can compute $\mathbf{x}_m^\perp$ directly from the right eigenvector $\mathbf{x}_m$.

4.6.1 2-D case

In Transverse Electric case, we have

$$\mathbf{E} = u\, \mathbf{e}_z, \quad \mathbf{H} = v_x\, \mathbf{e}_x + v_y\, \mathbf{e}_y.$$

We use a split formulation of the PMLs where $u = u_1 + u_2$ inside the PML. The unknowns u_1, u_2, and $\mathbf{v} = (v_x, v_y)$ are solutions of:

$$\begin{cases} -i\omega\, \varepsilon_b\, u_1 + \varepsilon_b\, \sigma_x\, u_1 - \dfrac{\partial v_x}{\partial x} = 0 \\ -i\omega\, \varepsilon_b\, u_2 + \varepsilon_b\, \sigma_y u_2 - \dfrac{\partial v_y}{\partial y} = 0 \\ -i\omega\mu_b\, \mathbf{v} + \mu_b \begin{pmatrix} \sigma_x & 0 \\ 0 & \sigma_y \end{pmatrix} \mathbf{v} - \nabla(u_1 + u_2) = 0 \\ u = 0 \quad \text{at the border of the PML.} \end{cases}$$

We consider the unknowns:

$$u = u_1 + u_2$$

$$u^* = u_1 - u_2.$$

u, u^*, v, are solutions of the following system,

$$\left\{\begin{array}{l} -i\omega\,\varepsilon_b\,u + \varepsilon_b\dfrac{\sigma_x+\sigma_y}{2}u + \varepsilon_b\dfrac{\sigma_x-\sigma_y}{2}u^* - \operatorname{div}\mathbf{v} \;=\; 0 \\ -i\omega\,\varepsilon_b\,u^* + \varepsilon_b\dfrac{\sigma_x+\sigma_y}{2}u^* + \varepsilon_b\dfrac{\sigma_x-\sigma_y}{2}u - \left(\dfrac{\partial v_x}{\partial x} - \dfrac{\partial v_y}{\partial y}\right) \;=\; 0 \\ -i\omega\mu_b\,\mathbf{v} + \mu_b\,\sigma\,\mathbf{v} - \nabla\,u \;=\; 0. \end{array}\right. \tag{32}$$

The unknown u^* exists only in the PML domain. In the physical domain, only unknowns u and $\mathbf{v}$ are present, and we solve

$$\left\{\begin{array}{l} -i\omega\,\varepsilon(\omega)\,u - \operatorname{div}\mathbf{v} \;=\; -i\omega j \\ -i\omega\mu_b\,\mathbf{v} + \mu_b\,\sigma\,\mathbf{v} - \nabla\,u \;=\; 0, \end{array}\right.$$

where j is the source term. Of course, additional unknowns p and q are added in Ω_{res} to linearize the system in ω. After discretization, we will obtain :

$$-i\omega\mathbf{M}_h\mathbf{U}_h + \mathbf{K}_h\mathbf{U}_h = \mathbf{F}_h.$$

The matrix $\mathbf{M}_h$ is symmetric, while $\mathbf{K}_h$ is not. The left eigenvector $\mathbf{x}_m^\perp$ and the right eigenvector $\mathbf{x}_m$ are written as:

$$\mathbf{x}_m^\perp = \begin{pmatrix} \mathbf{u}_m^\perp \\ \mathbf{u}_m^{*,\perp} \\ \mathbf{v}_m^\perp \end{pmatrix}, \quad \mathbf{x}_m = \begin{pmatrix} \mathbf{u}_m \\ \mathbf{u}_m^* \\ \mathbf{v}_m \end{pmatrix}.$$

We have obtained the following relations ($\lambda_m = i\tilde{\omega}_m$ is the eigenvalue associated with $\mathbf{x}_m$ and $\mathbf{x}_m^\perp$):

$$\mathbf{u}_m^\perp = \left(1 - \frac{\sigma_x+\sigma_y}{2\lambda_m}\right)\mathbf{u}_m$$

$$\mathbf{u}_m^{*,\perp} = \left(\frac{\sigma_x-\sigma_y}{2\lambda_m}\right)\mathbf{u}_m$$

and

$$\mathbf{v}_m^\perp = \left[\begin{array}{c} \dfrac{1}{\mu_b\,(-\lambda_m+\sigma_x)}\left(\dfrac{\partial\mathbf{u}_m^\perp}{\partial x} + \dfrac{\partial\mathbf{u}_m^{*,\perp}}{\partial x}\right) \\ \dfrac{1}{\mu_b\,(-\lambda_m+\sigma_y)}\left(\dfrac{\partial\mathbf{u}_m^\perp}{\partial y} - \dfrac{\partial\mathbf{u}_m^{*,\perp}}{\partial y}\right) \end{array}\right].$$

The proof is given in appendix B.

4.6.2 3-D case

In the PMLs we have:

$$\left\{\begin{array}{l} -i\omega\varepsilon_b\mathbf{E} + \varepsilon\mathbf{T}_{2,3,1}\mathbf{E} - \nabla\times\mathbf{H}^* = 0 \\ -i\omega\mu_b\mathbf{H} + \mu\mathbf{T}_{2,3,1}\mathbf{H} + \nabla\times\mathbf{E}^* = 0 \\ -i\omega\mathbf{E}^* + \mathbf{T}_{3,1,2}\mathbf{E}^* + i\omega\mathbf{E} - \mathbf{T}_{1,2,3}\mathbf{E} = 0 \\ -i\omega\mathbf{H}^* + \mathbf{T}_{3,1,2}\mathbf{H}^* + i\omega\mathbf{H} - \mathbf{T}_{1,2,3}\mathbf{H} = 0 \\ \mathbf{E}\times\mathbf{n} = 0 \quad \text{at the border of the PML,} \end{array}\right.$$

with $\mathbf{T}_{i,j,k} = \begin{pmatrix} \sigma_i & 0 & 0 \\ 0 & \sigma_j & 0 \\ 0 & 0 & \sigma_k \end{pmatrix}$. The unknowns $\mathbf{E}^*$ and $\mathbf{H}^*$ exist only in the PML domain. In the physical domain, there are only unknowns $\mathbf{E}$ and $\mathbf{H}$ (supplemented by unknowns $\mathbf{P}$ and $\mathbf{Q}$ in Ω_{res}) that solve (16). After discretization we will obtain:

$$-i\omega\mathbf{M}_h\mathbf{U}_h + \mathbf{K}_h\mathbf{U}_h = \mathbf{F}_h.$$

The matrices $\mathbf{M}_h$ and $\mathbf{K}_h$ are not symmetric (see appendix (C)). If we note $\mathbf{x}_m = (\mathbf{E}_m, \mathbf{H}_m, \mathbf{E}^*_m, \mathbf{H}^*_m)$ the right eigenvector, the left eigenvector $\mathbf{x}^\perp_m$ is given as:

$$\mathbf{x}^\perp_m = \begin{pmatrix} \mathbf{E}^*_m \\ -\mathbf{H}^*_m \\ \left(1 + \dfrac{\mathbf{T}_{2,3,1} - \mathbf{T}_{3,1,2}}{-\lambda_m + \mathbf{T}_{3,1,2}}\right)\varepsilon_b\mathbf{E}_m \\ -\left(1 + \dfrac{\mathbf{T}_{2,3,1} - \mathbf{T}_{3,1,2}}{-\lambda_m + \mathbf{T}_{3,1,2}}\right)\mu_b\mathbf{H}_m \end{pmatrix}. \tag{33}$$

The proof is given in appendix C. Straightforward computations give that

$$\langle \mathbf{M}_h\mathbf{x}_m, \mathbf{x}^\perp_m \rangle = \int_\Omega \frac{\partial(\tilde{\omega}_m\,\varepsilon(\tilde{\omega}_m))}{\partial\tilde{\omega}_m}\mathbf{E}_m\cdot\mathbf{E}_m - \frac{\partial\,(\tilde{\omega_m}\mu(\tilde{\omega}_m))}{\partial\tilde{\omega_m}}\,\mathbf{H}_m\cdot\mathbf{H}_m d\Omega$$

with

$$\varepsilon(\omega) = \varepsilon_b\frac{(-i\omega + \mathbf{T}_{2,3,1})\,(-i\omega + \mathbf{T}_{3,1,2})}{-i\omega\,(-i\omega + \mathbf{T}_{1,2,3})}, \quad \mu(\omega) = \mu_b\frac{(-i\omega + \mathbf{T}_{2,3,1})\,(-i\omega + \mathbf{T}_{3,1,2})}{-i\omega\,(-i\omega + \mathbf{T}_{1,2,3})}, \tag{34}$$

inside the PML. We find the announced normalization (11) in the introduction.

4.7 Static modes

In the 2-D transverse electric case ($\mathbf{E} = u\,\mathbf{e}_z$), the static modes satisfy

$$\nabla u_m = 0.$$

Moreover we impose a null Dirichlet condition on PML boundaries. As a result, the static modes satisfy $u_m = 0$ on all the domain. This is also true at a discrete level because u is discretized with continuous finite elements. As a result, static modes have non-null components mainly for unknown $\mathbf{v}$. The formulas (8), (9), (10), (14) and (28) can be used to reconstruct the unknown u if static modes are dropped.

For the 3-D case, the static modes satisfy

$$\nabla \times \mathbf{E}_m = 0.$$

They are usually constituted of gradients of functions. The associated eigenspace is usually large. In the numerical experiments, we have observed that 50% of the eigenmodes are static eigenmodes. Clearly, in large 3-D cases, it is not possible to compute and store all these static modes, that's why we have made the choice to compare formulas without these modes. Besides, we have observed that the matrix $\mathbf{M}_h^{-1}\mathbf{K}_h$ is often not diagonalizable because of these static modes. Because of this lack of diagonalization, some eigenvectors are not correctly computed or the Gram-Schmidt process fails.

5 Numerical results

The numerical results have been obtained with the software Montjoie Duruflé (2018) for the computation of finite element matrices $\mathbf{M}_h$ and $\mathbf{K}_h$ given in section 3. The fields will be displayed inside the physical domain.

In this section, all the eigenvalues of the matrix $\mathbf{M}_h^{-1}\mathbf{K}_h$ are computed with Lapack. We represent adimensionalized pulsations ω_m defined as

$$\omega_m = \frac{\tilde{\omega}_m}{\omega_{\text{adim}}}$$

where

$$\omega_{\text{adim}} = \frac{c_0}{L_0}, \quad L_0 = 10^{-7}.$$

c_0 is the speed of light and L_0 the characteristical length (here 100nm). All of the eigenvalues such that $|\omega_m| < 10^{-6}$ are dropped in order to remove static modes. Since the eigenvalues are complex conjugate, only eigenvalues (and associated eigenvectors) such that $\text{Re}(\tilde{\omega}_m) \geq 0$ are stored. The eigenvalues such that $\lambda_m = \sigma_i$ (σ_i is the damping function in PMLs) are also excluded, since the auxiliary fields $\mathbf{H}, \mathbf{E}^*, \mathbf{H}^*$ cannot be eliminated (division by zero) for these eigenvalues. In practice, we have observed that the associated eigenvectors have null components (at machine precision) for the unknown $\mathbf{E}_m$ and do not contribute to the field $\mathbf{E}_S$. Finally, if two pulsations ω_i, ω_j are close enough (i.e. $|\omega_i - \omega_j| < 10^{-6}$) they are considered degenerate.

In this section, we will compare the following formulas

- Formula (8) denoted as **Usual**, since it can be obtained from a direct linearization of Maxwell's equations.
- Formula (9) denoted as **Alternative Source**, since it can be obtained by choosing a different right hand side of Maxwell's equations.
- Formula (10) denoted as **Order2**, since it can be obtained from second-order formulation of Maxwell's equations.
- Formula (14) denoted as **P-unknown**, since it can be obtained by reconstructing the field $\mathbf{E}$ from the modal expansion of the unknown $\mathbf{P}$.
- Formula (28) denoted as **Q-unknown**, since it can be obtained with the unknown $\mathbf{Q}$.
- Formula (29) denoted as **Alternative + P**, since it can be obtained with the unknown $\mathbf{P}$ by choosing the alternative source. We observed that this formula does not work with metallic materials (an explanation is given in sub-section 4.4.1). As a result, this formula will be used for non-metallic materials only.

These formulas are rewritten in the table 1.

Table 1: Formulas used to computed the scattered field $\mathbf{E}_S$

With the coefficients α_m and β_m defined as

$$\beta_m = \frac{\omega}{(\tilde{\omega}_m - \omega)} \int_{\Omega_{res}} (\varepsilon(\omega) - \varepsilon_b)\mathbf{E}_{inc} \cdot \mathbf{E}_m d\Omega$$

$$\alpha_m = \int_{\Omega_{res}} (\varepsilon_b - \varepsilon_\infty)\mathbf{E}_{inc} \cdot \mathbf{E}_m d\Omega + \frac{\tilde{\omega}_m}{\tilde{\omega}_m - \omega} \int_{\Omega_{res}} (\varepsilon(\tilde{\omega}_m) - \varepsilon_b)\mathbf{E}_{inc} \cdot \mathbf{E}_m d\Omega$$

Formula	Expression
Formula (8) (Usual)	$\mathbf{E}_S = \sum \beta_m \mathbf{E}_m$
Formula (9) (Alternative Source)	$\mathbf{E}_S = \sum \alpha_m \mathbf{E}_m$
Formula (10) (Order2)	$\mathbf{E}_S = \sum \frac{\omega}{\tilde{\omega}_m} \beta_m \mathbf{E}_m$
Formula (14) (P-unknown)	$\mathbf{E}_S = \sum \frac{(\varepsilon(\tilde{\omega}_m) - \varepsilon_\infty)}{(\varepsilon(\omega) - \varepsilon_\infty)} \beta_m \mathbf{E}_m$
Formula (28) (Q-unknown)	$\mathbf{E}_S = \sum \frac{\tilde{\omega}_m}{\omega} \frac{(\varepsilon(\tilde{\omega}_m) - \varepsilon_\infty)}{(\varepsilon(\omega) - \varepsilon_\infty)} \beta_m \mathbf{E}_m$
Formula (29) (Alternative + P)	$\mathbf{E}_S = -\mathbf{E}_{inc} + \sum \frac{(\varepsilon(\tilde{\omega}_m) - \varepsilon_\infty)}{(\varepsilon(\omega) - \varepsilon_\infty)} \alpha_m \mathbf{E}_m$

5.1 2-D golden disk

In the 2-D case, we consider a scalar electric field (corresponding to the z-component of $\mathbf{E}_S$) and a vectorial magnetic field (corresponding to x and y-components of $\mathbf{H}_S$). We first look at the case of the field diffracted by a metallic disk with a radius of 100 nm, where the metal is gold, which can be can modeled accurately with Drude-Lorentz model (3) with $D = 2, L = 2$. We have chosen the values computed in (Sehmi et al., 2017b) (table II column with $L = 2$), they are repeated in table 2. These constants are given in electron-volts, they must be multiplicated

ε_∞	η_1	$\tilde{\gamma}_1$	η_2	$\tilde{\gamma}_2$
2.6585	1056.9	0	-1056.9	0.07247

σ_1	Ω_1	σ_2	Ω_2
0.57604 + 0.18443i	2.5509-0.27427i	4.1891+4.2426i	2.8685-1.2195i

Table 2: Constants ε_∞, η_k, $\tilde{\gamma}_k$, σ_k, Ω_k for gold.

by $\dfrac{2\pi e}{h}$ where $e = 1.602176634 \cdot 10^{-19}$ is the elementary charge and $h = 6.62607015 \cdot 10^{-34}$ is the Planck constant. The physical computation domain is 400 nm long and 200 nm wide (see figure 1). PML layers are added to the mesh of figure 1. The thickness of PML is equal to 100nm with two cells in direction of PMLs. The damping of PMLs σ is taken equal to 3. The disk is made of gold while the surrounding medium is the vacuum. We represent in figure 2

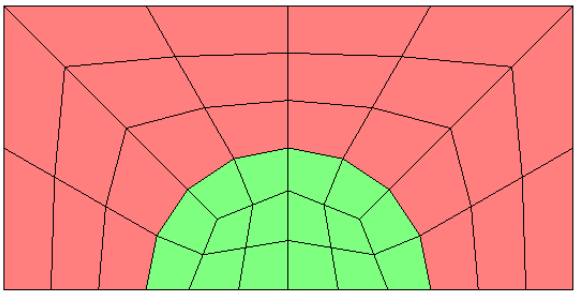

Figure 1: Mesh used for the scattering of a disk

the numerical adimensionalized pulsations ω_m obtained with the mesh displayed in figure 1 and fourth-order finite elements. We can compare these pulsations with analytical QNMs for the disk (computed with Bessel functions). The comparison is displayed in figure 3. We see that QNMs are correctly computed, and we also observe the presence of other modes that we call PML modes. The matrices $\mathbf{M}_h$ and $\mathbf{K}_h$ have 6440 rows. Among the 2364 eigenvectors stored, 488 are associated with a degenerate eigenvalue. Degenerate eigenvalues are represented with red squares in figure 2. These degenerate eigenvalues are due to accumulation points (here due to poles of the dielectric permittivity) or due to PML layers.

The field driving the system is a plane wave propagating along the x-axis, at the real frequency ω :

$$\mathbf{E}_{\text{inc}} = e^{ikx}\mathbf{e}_z$$

where $k = \dfrac{\omega}{c_0}$ is the wave number. The scalar field $u = E_z$ is discretized with continuous finite elements (here $\mathbb{Q}_4$ with the mesh of figure 1). The solution is plotted for two wavelengthes

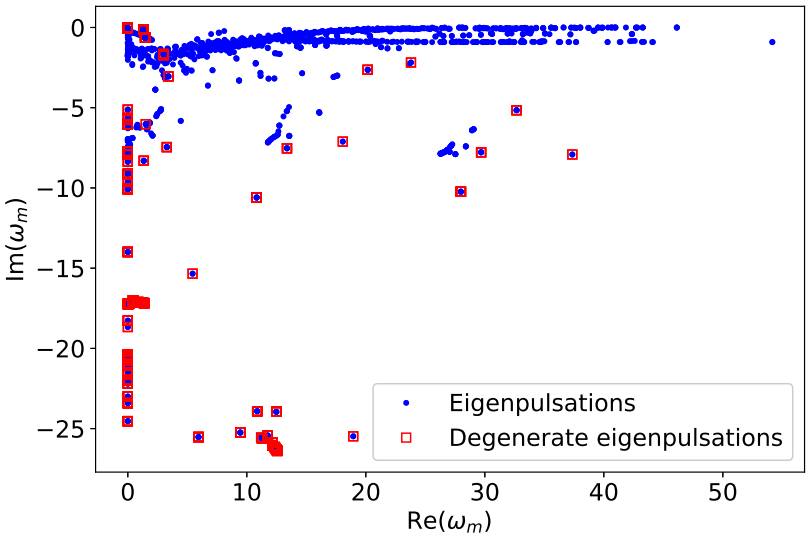

Figure 2: All numerical adimensionaliazed eigenvalues for the golden disk, degenerate eigenvalues are located within red squares.

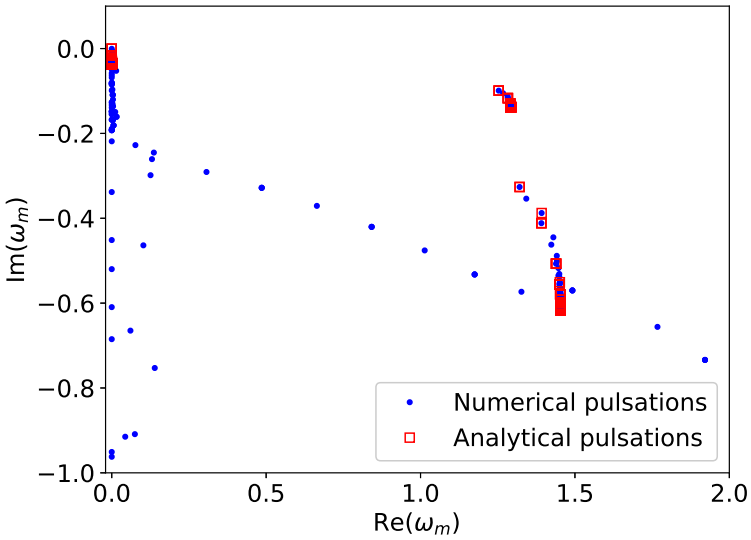

Figure 3: Numerical eigenvalues located in the box $[0, 2] \times [-1, 0]$ for the golden disk. In red, analytical eigenvalues of Quasi Normal Modes.

$\lambda = 250nm$ and $\lambda = 500nm$ in figure 4. In this figure, we represent the solution only inside the physical domain (without PMLs). For the wavelength $\lambda = 250nm$, we have computed a relative L^2 error of 0.094% between the numerical solution and the analytical solution (computed with

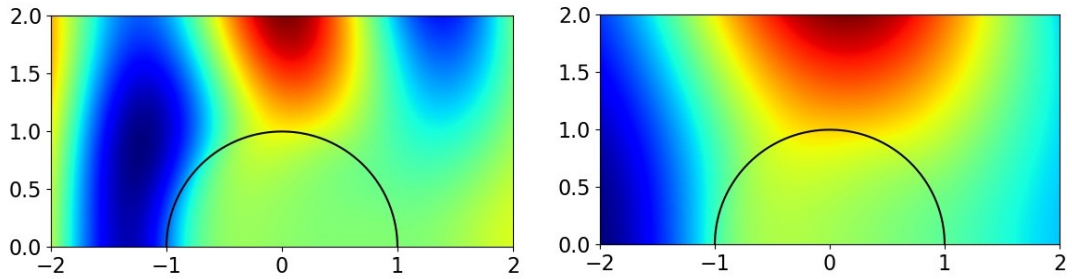

Figure 4: Real part of the total field for $\lambda = 250nm$ and $\lambda = 500nm$ and the golden disk.

Hankel functions).

We compute the field diffracted by the disk for 201 angular frequencies ω evenly spaced in the interval $[\omega_1, \omega_2]$ where

$$\omega_1 = \frac{2\pi c_0}{\lambda_1}, \quad \omega_2 = \frac{2\pi c_0}{\lambda_2}.$$

The two wavelengthes λ_1, λ_2 are equal to 1 μm and 250 nm. In figure 5, we display the relative error between the modal solution

$$\mathbf{E}_S^{\text{modal}} = \sum_m \alpha_m \tilde{\mathbf{E}}_m$$

and the direct FEM solution

$$\mathbf{E}_S^{FEM} = (-i\omega \mathbf{M}_h + \mathbf{K}_h)^{-1} \mathbf{F}_h$$

as a function of the spectrum width. For a given spectral width, the relative error is computed for the 201 angular frequencies and the maximum value of this error is retained and plotted. For a given spectral width L, only the modes whose eigenfrequencies $\tilde{\omega}_m$ verify

$$\text{Re}(\tilde{\omega}_m) \in [-L\,\omega_{\text{adim}}, L\,\omega_{\text{adim}}] \,\text{and}\, \text{Im}(\tilde{\omega}_m) \in [-\omega_{\text{adim}} L/2, 0]$$

are included in the expansion. The relative error is computed on the whole physical domain Ω_p (PMLs are not included) by the formula

$$\text{Relative Error} = \sqrt{\frac{\int_{\Omega_p} \left| \mathbf{E}_S^{\text{modal}} - \mathbf{E}_S^{FEM} \right|^2 d\Omega_p}{\int_{\Omega_p} \left| \mathbf{E}_S^{FEM} \right|^2 d\Omega_p}}$$

For this case, all the formulas converge nicely to the expected solution. The formula (14) is the most accurate while the formula (8) is the least accurate.

5.2 2-D silicon square

We consider the scattering by a silicon square $[-400nm, 400nm]^2$ surrounded by vacuum. The computational domain is a rectangle $[-500nm, 500nm] \times [0, 500nm]$. A Neumann condition is imposed on the axis of symmetry $y = 0$. The silicon is modeled by a Lorentz model with five poles as proposed in Sehmi et al. (2017a), the values for Ω_k and σ_k are repeated in table 3. The

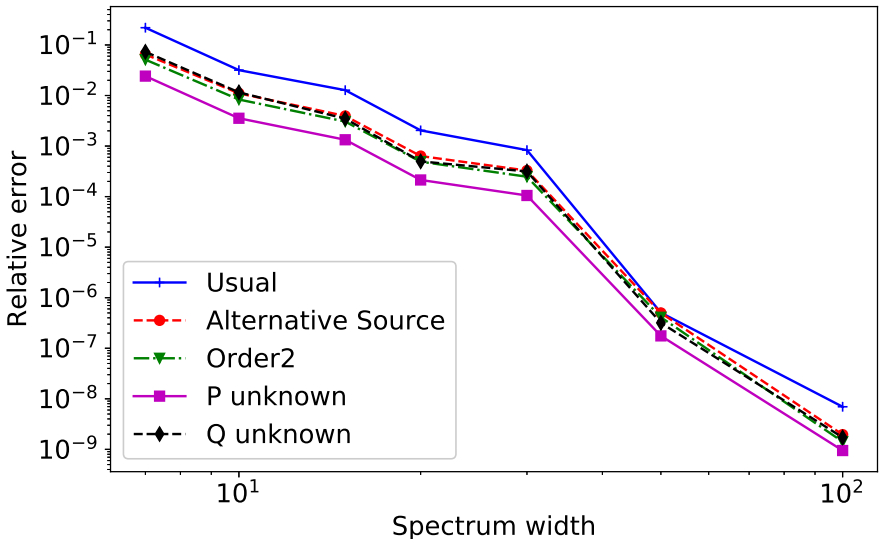

Figure 5: Relative error between the scattered field computed with the modal expansion and with a direct FEM solver as a function of the spectral width. Case of the golden disk.

ε_∞	σ_1	Ω_1	σ_2	Ω_2	σ_3
0.81568	1.6934 + 2.084i	3.3736 - 0.11402i	5.2573 + 8.0106i	3.6519 - 0.52378i	-1.7164 + 5.9939i

Ω_3	σ_4	Ω_4	σ_5	Ω_5
4.287 - 0.21116i	-0.00528 + 0.32911i	5.3188 - 0.18434i	-3.8438 + 6.9298i	5.5064 - 1.7892i

Table 3: Constants ε_∞, σ_k, Ω_k for silicon.

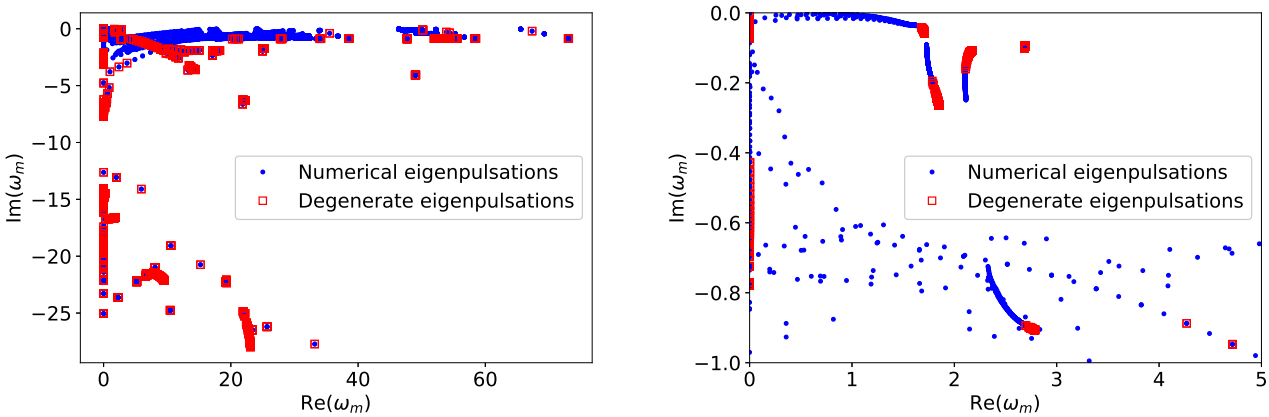

Figure 6: All numerical adimensionaliazed eigenvalues for the silicon square, degenerate eigenvalues are located within red squares. On the right, eigenvalues contained in the box $[0, 5] \times [-1, 0]$.

thickness of PML is equal to 100nm with one cell in direction of PMLs. The damping of PMLs σ is taken equal to 3. Eighth-order finite elements are used for this simulation. In figure 6, the eigenpulsations ω_m are plotted in the complex plane. We see the accumulation points (with their multiple eigenvalues) that are located on poles of $\varepsilon(\omega)$. The matrices $\mathbf{M}_h, \mathbf{K}_h$ contain 39640

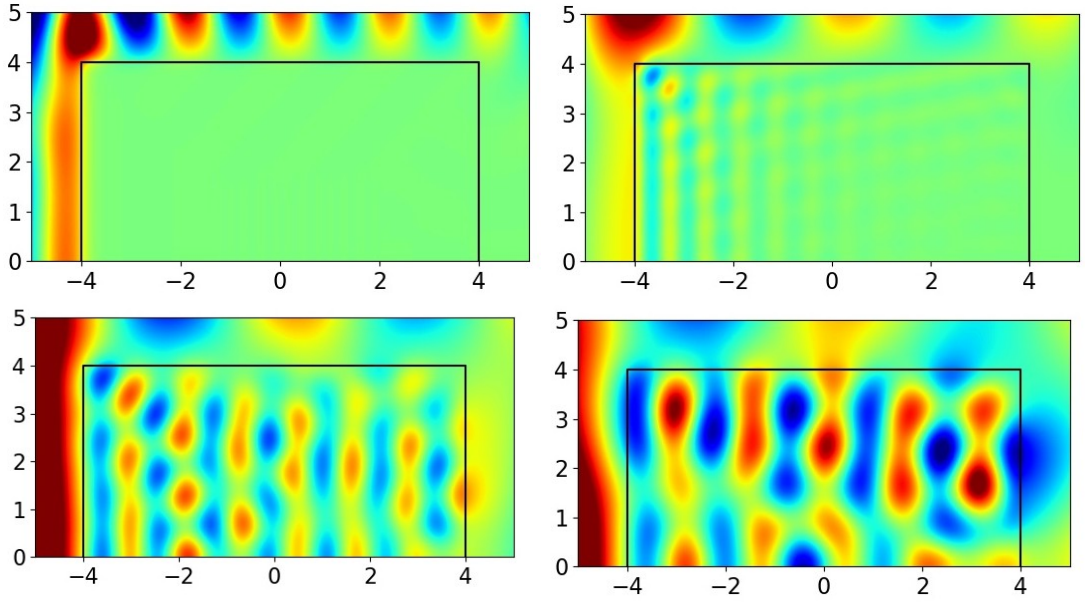

Figure 7: Real part of the total field for wavelengthes $\lambda = 200nm, 400nm, 500nm, 600nm$ for the silicon square (left to right and top to bottom).

rows. Among the 16933 eigenvectors stored, 4974 are associated with a degenerate eigenvalue. The field driving the system is a plane wave propagating along the x-axis, at the real frequency ω :

$$\mathbf{E}_{\text{inc}} = e^{ikx}\mathbf{e}_z$$

The total field is displayed in 7 for different wavelengthes. We see the change of behavior of silicon. This material has almost no damping for $\lambda > 500nm$ and behaves almost like a metal for short wavelengthes.

In figure 8, we chose to represent the error inside the silicon resonator in order to compare the formula (29) with other formulas. The relative error is computed for 201 angular frequencies and the maximum value of this error is retained. Pulsations are evenly spaced in the interval $[\omega_1, \omega_2]$ where

$$\omega_1 = \frac{2\pi c_0}{\lambda_1}, \quad \omega_2 = \frac{2\pi c_0}{\lambda_2}.$$

The two wavelengthes λ_1, λ_2 are equal to 800 mm and 200 nm. We observed that the formula (29) does not work outside the resonator, but provides accurate results inside the resonator. For this case, the formula (8) is the least accurate. The large number of modes N is here due to the presence of accumulation points in the region of interest (five poles). Finally, in figure 9, the relative L^2 error inside the square is plotted versus the angular frequency ω when $N = 8908$ modes are used in the modal expansion.

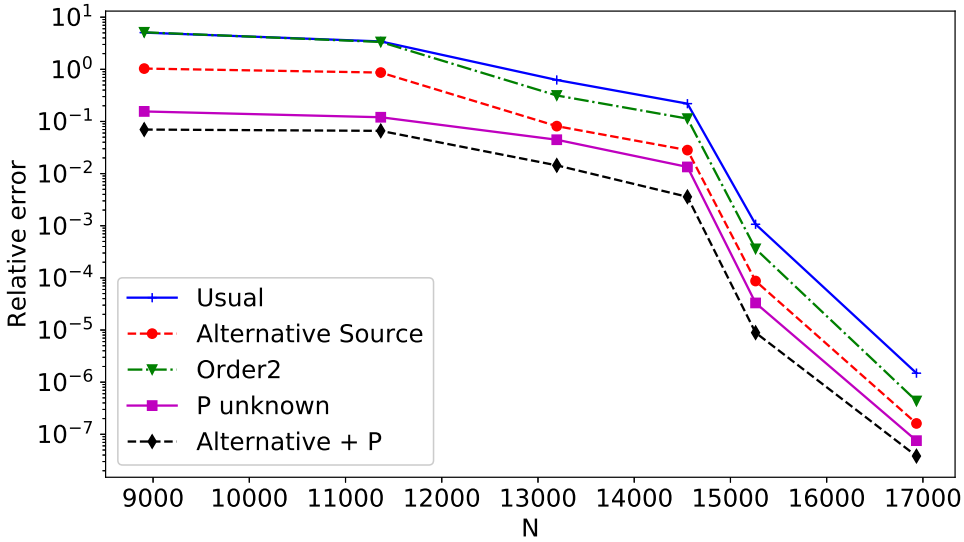

Figure 8: Relative L^2 error for the interior of the silicon square versus the number of modes N.

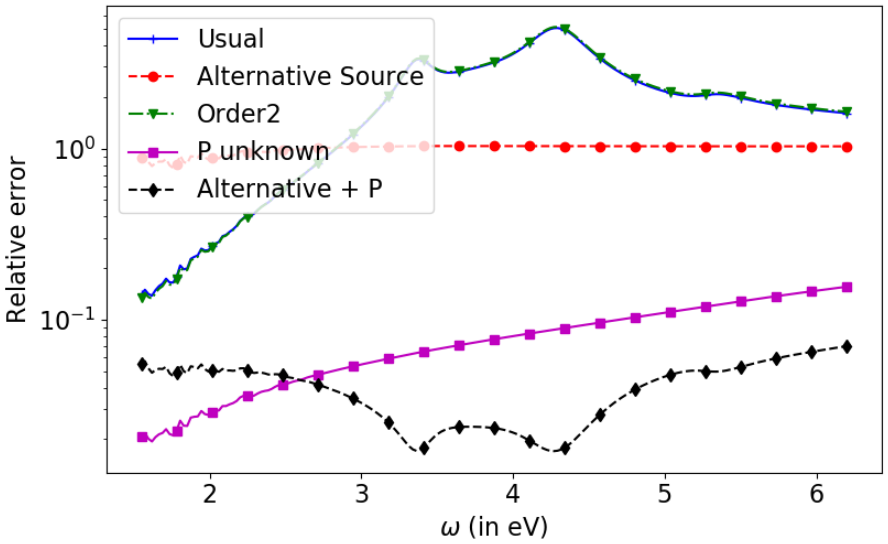

Figure 9: Relative L^2 error versus the pulsation ω for the interior of the silicon square

5.3 3-D silicon sphere

We consider the case of a field diffracted by a silicon sphere with a radius of 100 nm. The silicon can be modeled accurately for $\lambda \in [500\ nm, 1.5\ \mu m]$ by a Drude-Lorentz model with a single pole ($D = 0, L = 1$). The coefficients Ω_k and σ_k are found by a least-squares fitting over the interval

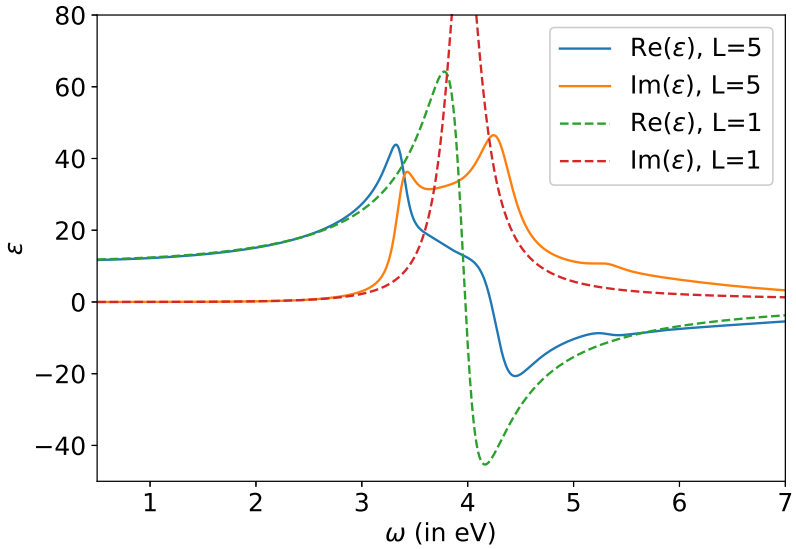

Figure 10: Real part and imaginary part of $\varepsilon(\omega)$ for a Lorentz model of the silicon with one pole ($L = 1$) or five poles ($L = 5$).

[500 nm, 1.5 μm] by using the function *least_squares* of Python package scipy.optimize. The obtained coefficients are given in table 4. The constants σ_1 and Ω_1 are given in electron-volts. In

ε_∞	σ_1	Ω_1
1.12648273	2.1759525332+20.775848892i	3.95095351-0.19089288i

Table 4: Constants ε_∞, σ_k, Ω_k for silicon.

figure 10, the permittivity has been represented for this reduced model ($L = 1$) and the original model given by table 3 ($L = 5$). We check that there is a good agreement until $\omega \approx 2.5eV$ which corresponds to wavelengthes greater than 500 nm. The physical computation domain is the parallelepiped box $[0, 150nm] \times [0, 150nm] \times [-150nm, 150nm]$ with a quarter of the dielectric ball (see figure 11). PML layers are added to the mesh of figure 11. The thickness of PML is equal to 100nm with only one cell in direction of PMLs. The damping of PMLs σ is taken equal to 1. The source is an incident plane wave oriented in z-direction and polarized in x-direction

$$\mathbf{E}_{\text{inc}} = e^{ikz}\mathbf{e}_x$$

We impose a Perfectly conducting condition on plane $x = 0$ (i.e. $\mathbf{E} \times n = 0$) and a Neumann condition on plane $y = 0$ (i.e. $\mathbf{H} \times n = 0$) in order to have the same solution as for the whole sphere. Fourth order edge elements are used for the unknown $\mathbf{E}$ and the mesh of figure 11. We compute the field diffracted by the sphere for 201 angular frequencies ω evenly spaced in the interval $[\omega_1, \omega_2]$ where

$$\omega_1 = \frac{2\pi c_0}{\lambda_1}, \quad \omega_2 = \frac{2\pi c_0}{\lambda_2}.$$

The two wavelengthes λ_1, λ_2 are equal to 1.5 μm and 500 nm. The numerical solution obtained for 500nm is plotted in figure 12. The error between this solution and the analytical solution

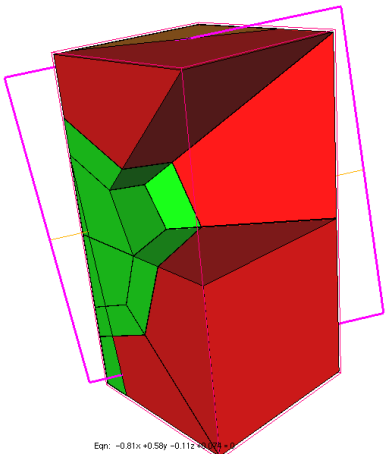

Figure 11: Mesh used for the scattering of a sphere

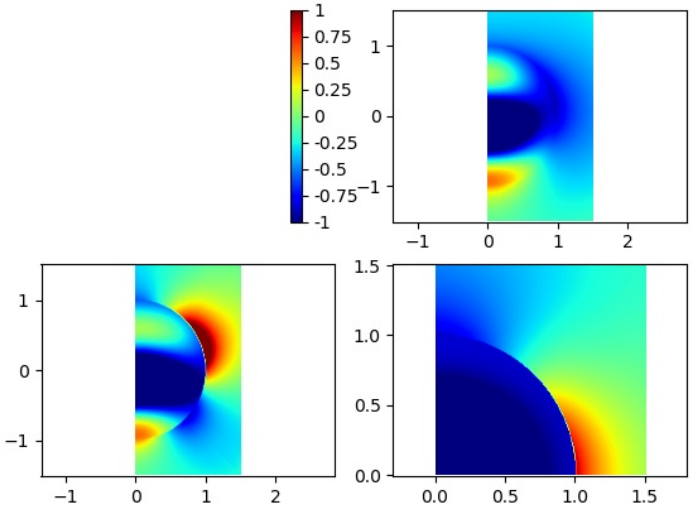

Figure 12: Real part of diffracted field (component E_x of electric field) for three planes Oxy, Oxz and Oyz. Case of a silicon sphere ($\lambda = 500$ nm).

computed with Mie's series is equal to 1.3% for 500nm and 3% for 1.5 μm. For this case, the matrices $\mathbf{M}_h, \mathbf{K}_h$ have 31 246 rows. Among the 8084 stored eigenvectors, 817 are associated with degenerate eigenvalues.

Numerical pulsations are plotted in figure 13 with the same adimensionalization coefficient ω_{adim} as in 2-D. When we zoom in on the box $Re(\omega) \in [0, 5\,\omega_{\text{adim}}], Im(\omega) \in [-0.5\,\omega_{\text{adim}}, 0.0]$, we obtain pulsations ω_m of the figure 14. In this figure, we have also represented the analytical pulsation of QNMs. Similarly to the 2-D case, we compute the relative error between the modal solution and the direct FEM solution. However, the relative error is computed with the curl of

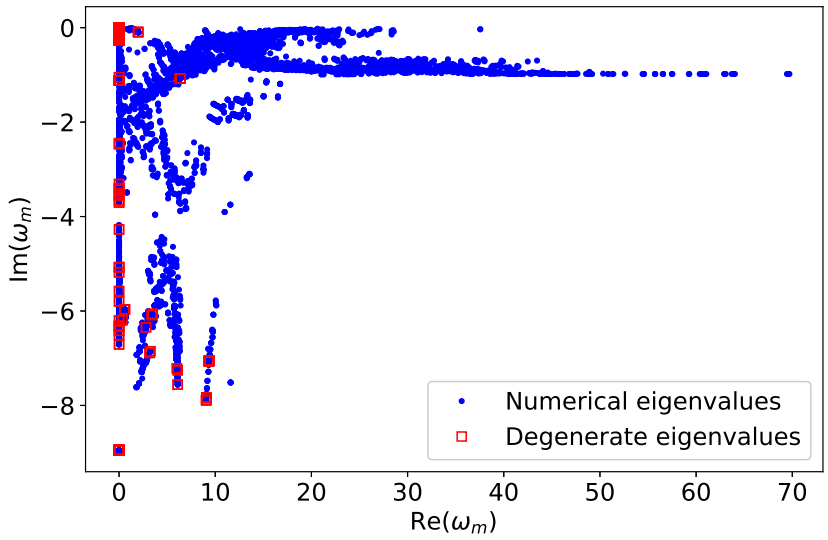

Figure 13: Numerical adimensionalized pulsations for the silicon sphere. Degenerate eigenvalues are located within red squares.

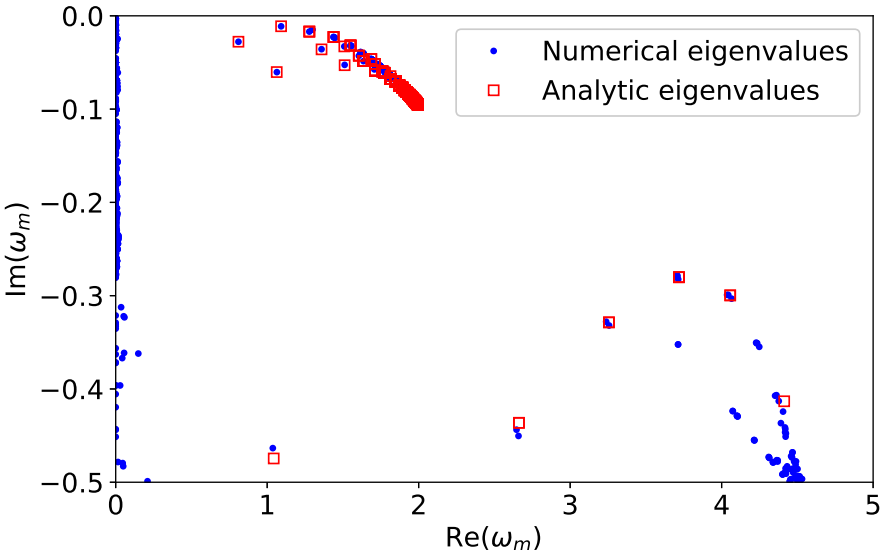

Figure 14: Numerical adimensionalized pulsations for the silicon sphere. Numerical eigenvalues are in blue, analytical QNMs in red.

E in order to remove the contribution of static modes:

$$\text{Relative Error} = \sqrt{\frac{\int_{\Omega_p} \left| \nabla \times \mathbf{E}_S^{\text{modal}} - \nabla \times \mathbf{E}_S^{FEM} \right|^2 d\Omega_p}{\int_{\Omega_p} \left| \nabla \times \mathbf{E}_S^{FEM} \right|^2 d\Omega_p}}$$

This error is plotted in figure 15 for different formulas. Similarly to what has been observed

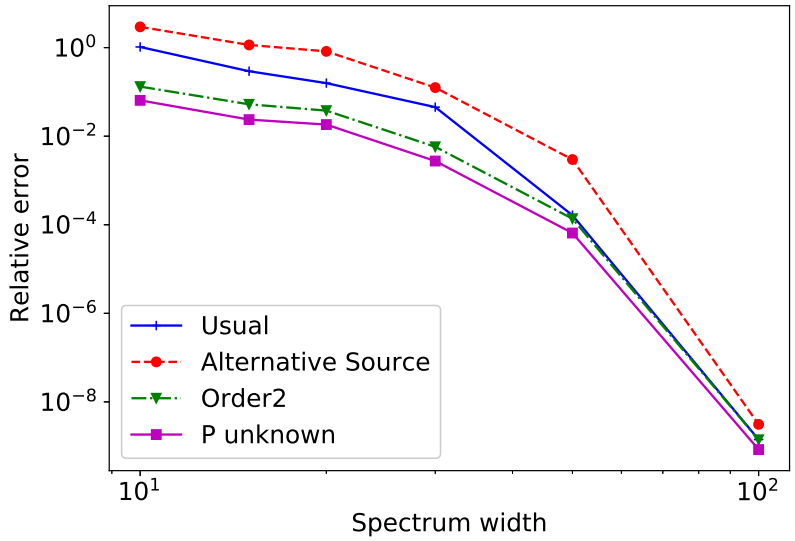

Figure 15: Relative error on curl of E versus the spectral width. Case of the silicon sphere.

in 2-D, the formulas provide a modal solution that converges towards the direct FEM solution. For this case, the formula (14) is the most accurate while the formula (9) is the least accurate. Similarly to the 2-D case, only modes such that

$$\mathrm{Re}(\tilde{\omega}_m) \in [-L\,\omega_{\mathrm{adim}}, L\,\omega_{\mathrm{adim}}] \,\mathrm{and}\, \mathrm{Im}(\tilde{\omega}_m) \in [-\omega_{\mathrm{adim}} L/2, 0]$$

are kept, where L is the spectral width. When a reduced spectrum is selected, the formula (14) is the most accurate. In figure 16, the relative error is computed on curl($\mathbf{E}$) but only inside the resonator. We can see that the formula (29) is quite accurate for small values of L, this formula does not converge because the incident field is projected on degrees of freedom by interpolation (instead of solving a linear system with the mass matrix). As a result, it stagnates at 1 % which is the level of accuracy of the interpolation for this case.

If the electric field is desired, a nice approach consists in discretizing $\mathbf{H}$ with edge elements (instead of $\mathbf{E}$), reconstructing $\mathbf{H}$ with the modal expansion:

$$\mathbf{H}^{\mathrm{modal}} = \sum \alpha_m \tilde{\mathbf{H}}_m.$$

and of computing $\mathbf{E}_S$ by using Maxwell's equations

$$\mathbf{E}_S = \frac{1}{-i\omega\varepsilon(\omega)} \left(\mathbf{J} + \nabla \times \mathbf{H}^{\mathrm{modal}} \right) \tag{35}$$

In figure 17, the relative error on the electric field has been computed by using this method. The formulas (8), (9), (14) or (28) can be used to obtain $\mathbf{H}^{\mathrm{modal}}$ with the coefficients α_m (because they are obtained with $\mathbf{f}_2 = 0$, see for instance theorem 5). The coefficients α_m given by the formula (10) can be used only to reconstruct $\mathbf{E}^{\mathrm{modal}}$ (with equation (15)). The reason is that

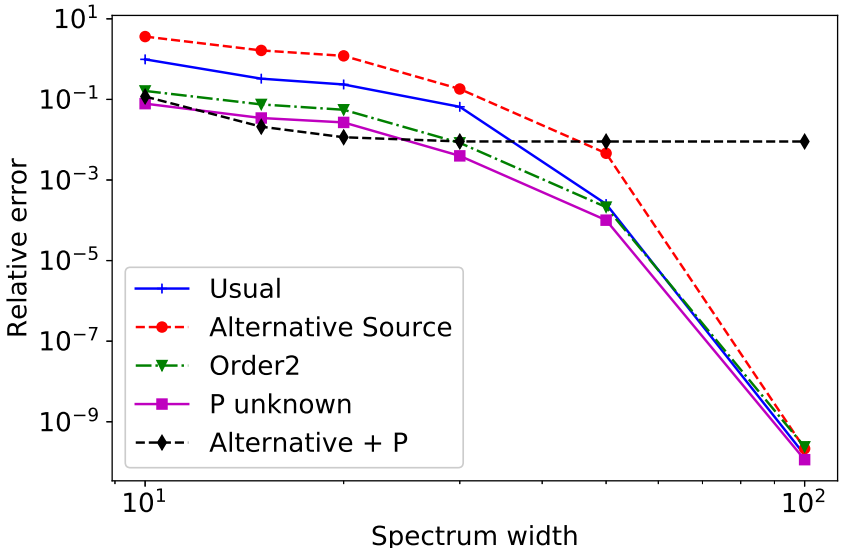

Figure 16: Relative error on curl of $\mathbf{E}_S$ versus the spectral width. Case of the silicon sphere, only interior of the sphere is taken into account.

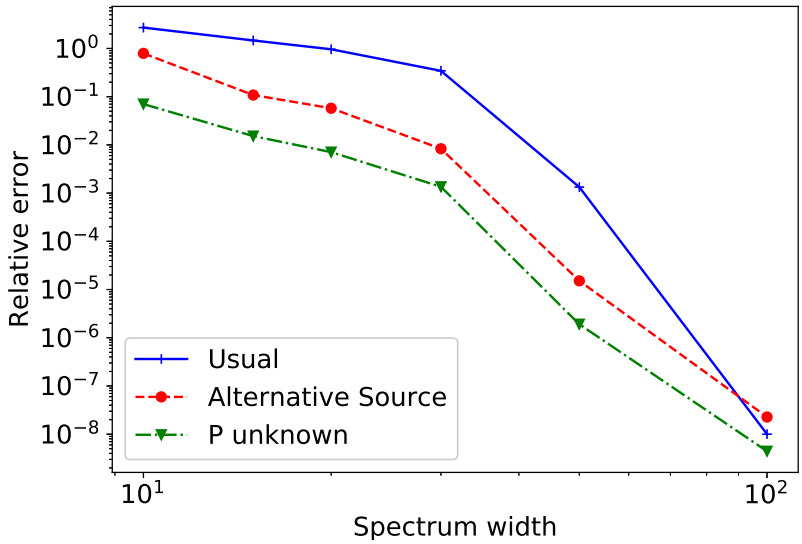

Figure 17: Relative error on electric field $\mathbf{E}_S$ (as computed in (35)) versus the spectral width. Case of the silicon sphere.

this formula has been established by introducing the unknowns $\mathbf{E}, \mathbf{E}', \mathbf{P}', \mathbf{Q}'$ (see section (4.3)). Thus, only these four unknowns can be reconstructed with this formula and not $\mathbf{H}$. In figure 17, we observe that the reconstructed field $\mathbf{E}$ with this method converges correctly to the numerical

eletrical field. For this case, the formula (14) is the most accurate.

5.4 Silver rod

We consider the case of a silver rod. The resonator is a cylinder of radius 240 nm and of height 400 nm. Only a quarter of the cylinder is meshed with Dirichlet/Neumann conditions to obtain the same solution as for the full cylinder. PML layers are added for $x, y, z > 400nm$ and a Silver-Müller condition is set for $z = -400nm$. The silver material is modeled by a Drude-Lorentz model with $D = 2, L = 2$. In table 5, coefficients of this model are given, they have obtained with the function *least_ square* as in the previous function. The measured values of ε have been taken from `http://sspectra.com/sopra.html`. In figure 18, we have represented the

ε_∞	η_1	$\tilde{\gamma}_1$	η_2	$\tilde{\gamma}_2$
1.2135	883.46	0	-883.46	0.0866887

σ_1	Ω_1	σ_2	Ω_2
3.5366 + 4.5884i	4.249 - 2.1153i	0.74248e - 0.19950i	4.0097 - 0.30102i

Table 5: Constants ε_∞, η_k, $\tilde{\gamma}_k$, σ_k, Ω_k for silver.

measured $\varepsilon(\omega)$ and the computed model. Fourth-order edge elements are used, the numerical

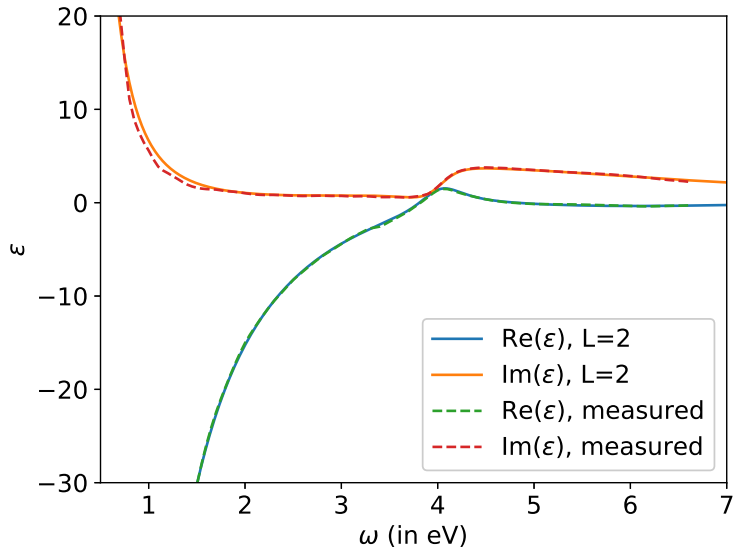

Figure 18: Real and imaginary part of ε versus ω. Comparison between the measured permittivity and the Drude-Lorentz model.

eigenpulsations obtained for this case are displayed in figure 19. The matrices $\mathbf{M}_h, \mathbf{K}_h$ have 36 089 rows. Among the 9836 stored eigenvectors, we have 486 eigenvectors associated with a degenerate eigenvalue. For this case, we observe in figure 19 that degenerate eigenvalues appear only for poles and zeros of the permittivity $\varepsilon(\omega)$. Degenerate eigenvalues associated with PMLs appear most of the time because of the symmetry of the PML layout. For example, if we replace

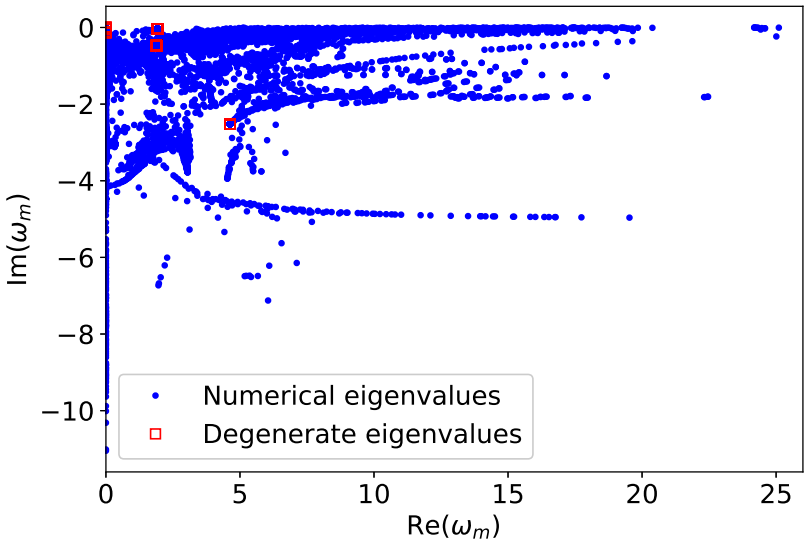

Figure 19: Numerical eigenpulsations ω_m in the complex plane for the silver rod.

the Silver-Müller condition by a PML for $z < -400nm$ with the same parameters as for the PML $z > 400nm$ (i.e. same damping σ and same thickness), degenerate eigenvalues are observed outside of poles and zeros of $\varepsilon(\omega)$.

The source is an incident plane wave oriented in z-direction and polarized in x-direction

$$\mathbf{E}_{\text{inc}} = e^{ikz}\mathbf{e}_x$$

We compute the field diffracted by the sphere for 201 angular frequencies ω evenly spaced in the interval $[\omega_1, \omega_2]$ where

$$\omega_1 = \frac{2\pi c_0}{\lambda_1}, \quad \omega_2 = \frac{2\pi c_0}{\lambda_2}.$$

The two wavelengthes λ_1, λ_2 are equal to 900 nm and 400 nm. With this choice of wavelengthes, the real part of the permittivity does not belong to the critical interval $\left[-3, -\frac{1}{3}\right]$. The mesh is very coarse, such that the numerical solution (see figure 20) is not accurate. The numerical error is estimated to be around 20 %. In figure 21, the different formulas are compared in the physical domain. We observe that the formula (14) is the most accurate for this case.

6 Conclusion

In this report, we have considered the solution of Maxwell's equations for dispersive materials modeled by a Drude-Lorentz model. A classical approach to compute the solution on a frequency range consists of computing the eigenmodes of the system (QNMs) and projecting the solution on these modes. We have shown how different linearizations of Maxwell's equations with respect to the pulsation ω can lead to several formulas for the projection coefficients α_m. With this approach, we show how formulas classically found in the literature (e.g. (8), (9), (10)) can be

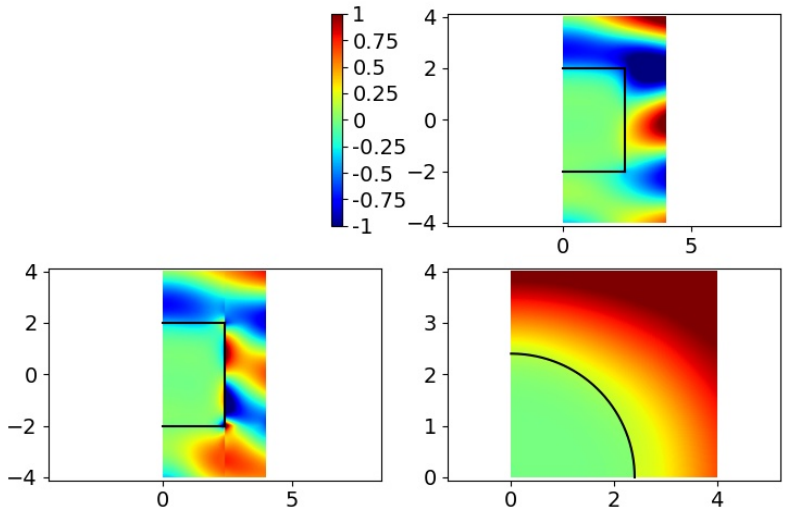

Figure 20: Real part of the total field (component E_x of electric field) for three planes Oxy, Oxz and Oyz. Case of a silver rod ($\lambda = 400$ nm).

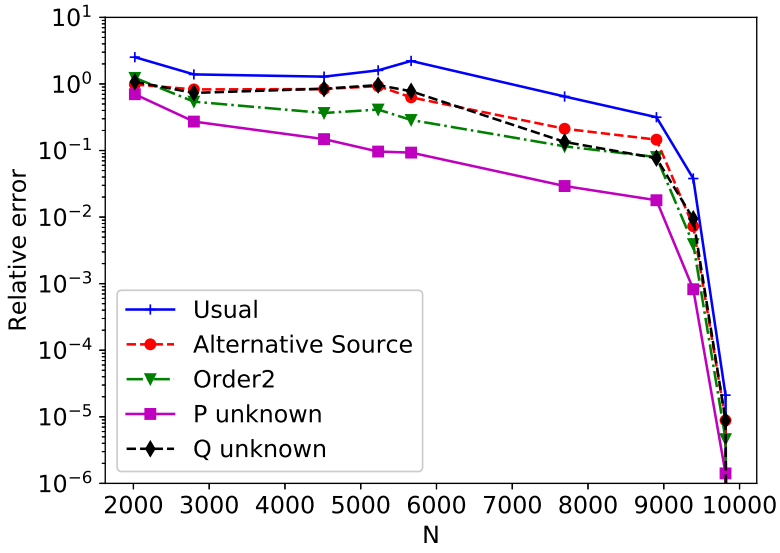

Figure 21: Relative error on curl of $\mathbf{E}_S$ versus the number of modes N. Case of the silver rod.

proven at a discrete level. An infinity of formulas exist for the excitation coefficients α_m, a general formula (12) is obtained by splitting the source into the different equations. The formulas (14), (30) and (28)) are obtained with a particular choice of splitting. We have established the link between the biorthogonal projection (that is usually the method of choice in numerics to project

the solution on eigenvectors) and analytic formulas that have been obtained in the continuous space. Because of the symmetry of Maxwell's equations, the left eigenvector can be computed from the right eigenvector without solving the transpose eigenvalue problem. The expressions of the left eigenvectors are provided by the theorem (1) for Drude-Lorentz material and by the equation (33) for dispersive PMLs. We provided in the algorithm 1 a simple way to handle correctly degenerate eigenvalues. These eigenvalues usually appear because of accumulation points (located at poles or zeros of the permittivity function) or because of a symmetry in the PML layout.

Numerical experiments confirm that the formulas (8), (9), (10), (14), (30) and (28) can be used to reconstruct the electric field. If all the eigenmodes are included in the modal expansion, all these formulas provide the same solution, i.e. the finite element solution. In the tested cases, the formula (14) is the most accurate. In the case of non-metallic resonators ($\omega_{0,k} \neq 0$), the formula (29) is of interest to obtain the field inside the resonator. In 3-D computations, since static modes are dropped, the electric field cannot be computed directly (only its curl is correctly computed). We have proposed to use formulas (8), (9), (14) or (28) to compute the magnetic field and recover the electric field by using Maxwell's equations (equation (35)).

References

Abdelrahman, M. I. and Gralak, B. (2018). Completeness and divergence-free behavior of the quasi-normal modes using causality principle. OSA Continuum, 1(2):340–348.

Bai, Q., Perrin, M., Sauvan, C., Hugonin, J.-P., and Lalanne, P. (2013). Efficient and intuitive method for the analysis of light scattering by a resonant nanostructure. Opt. Express, 21(22):27371–27382.

Binkowski, F., Zschiedrich, L., and Burger, S. (2019). An auxiliary field approach for computing optical resonances in dispersive media. J. Eur. Opt. Soc.-Rapid Publ.

Cohen, G. and Duruflé, M. (2007). Non spurious spectral-like element methods for Maxwell's equations. Journal of Computational Mathematics, 25:282–304.

Colom, R., Mcphedran, R., Stout, B., and Bonod, N. (2018). Modal expansion of the scattered field: Causality, nondivergence, and nonresonant contribution. Physical Review B : Condensed matter and materials physics, 98:085418.

Duruflé, M. (2018). Montjoie webpage. `http://montjoie.gforge.inria.fr/`.

Lalanne, P., Yan, W., Gras, A., Sauvan, C., Hugonin, J.-P., Besbes, M., Demésy, G., Truong, M. D., Gralak, B., Zolla, F., Nicolet, A., Binkowski, F., Zschiedrich, L., Burger, S., Zimmerling, J., Remis, R., Urbach, P., Liu, H. T., and Weiss, T. (2019). Quasinormal mode solvers for resonators with dispersive materials. J. Opt. Soc. Am. A, 36(4):686–704.

Lalanne, P., Yan, W., Vynck, K., Sauvan, C., and Hugonin, J.-P. (2018). Light interaction with photonic and plasmonic resonances. Laser & Photonics Reviews, page 1700113.

Muljarov, E. A. and Langbein, W. (2016). Resonant-state expansion of dispersive open optical systems: Creating gold from sand. Phys. Rev. B, 93:075417.

Sauvan, C., Hugonin, J. P., Maksymov, I. S., and Lalanne, P. (2013). Theory of the spontaneous optical emission of nanosize photonic and plasmon resonators. Phys. Rev. Lett., 110:237401.

Sehmi, H. S., Langbein, W., and Muljarov, E. A. (2017a). Optimizing the Drude-Lorentz model for material permittivity: Examples for semiconductors.

Sehmi, H. S., Langbein, W., and Muljarov, E. A. (2017b). Optimizing the Drude-Lorentz model for material permittivity: Method, program, and examples for gold, silver, and copper. Phys. Rev. B, 95:115444.

Vial, B., Zolla, F., Nicolet, A., and Commandré, M. (2014). Quasimodal expansion of electromagnetic fields in open two-dimensional structures. Phys. Rev. A, 89:023829.

Wooten, F. (1972). Optical Properties of Solids. Academic Press.

Wu, T., Baron, A., Lalanne, P., and Vynck, K. (2019). Intrinsic multipolar contents of nanoresonators for tailored scattering. arXiv:1907.04598.

Yan, W., Faggiani, R., and Lalanne, P. (2018). Rigorous modal analysis of plasmonic nanoresonators. Phys. Rev. B, 97:205422.

Zimmerling, J., Wei, L., Urbach, P., and Remis, R. (2016). A Lanczos model-order reduction technique to efficiently simulate electromagnetic wave propagation in dispersive media. J. Comput. Phys., 315:348–362.

Zolla, F., Nicolet, A., and Demésy, G. (2018). Photonics in highly dispersive media: the exact modal expansion. Opt. Lett., 43(23):5813–5816.

Zschiedrich, L., Binkowski, F., Nikolay, N., Benson, O., Kewes, G., and Burger, S. (2018). Riesz-projection-based theory of light-matter interaction in dispersive nanoresonators. Phys. Rev. A, 98:043806.

A Finite element matrices

A.1 First-order formulation

The computational domain Ω is made of hexahedra (in 3-D) :

$$\Omega = \bigcup K_i$$

where K_i is a single hexahedron. Edge elements based on Nédélec's first family are used for the unknowns $\mathbf{E}$ and discontinuous finite elements for unknowns $\mathbf{H}$, $\mathbf{P}$ and $\mathbf{Q}$:

$$\mathbf{E} \in \mathbf{V}_h = \left\{ \mathbf{u} \in H(\mathrm{curl}, \Omega) \text{ such that } \forall K_i \in \Omega, \quad DF_i^T \mathbf{u} \circ F_i \in \mathbb{Q}_{r-1,r,r} \times \mathbb{Q}_{r,r-1,r} \times \mathbb{Q}_{r,r,r-1} \right\}$$

$$\mathbf{H}, \mathbf{P}, \mathbf{Q} \in \mathbf{W}_h = \left\{ \mathbf{u} \in (L^2(\Omega))^3 \text{ such that } \forall K_i \in \Omega, \quad \mathbf{u} \in \mathbb{Q}_{r,r,r}^3 \right\}$$

where F_i is the transformation from the unit cube $[0,1]^3$ to the hexahedron K_i, DF_i its jacobian matrix and $\mathbb{Q}_{r_1,r_2,r_3}$ is the following polynomial space

$$\mathbb{Q}_{r_1,r_2,r_3} = \left\{ p(\mathbf{x}) = \sum_{\ell=0}^{r_1} \sum_{m=0}^{r_2} \sum_{m=0}^{r_3} a_{\ell,m,n}\, x_1^\ell x_2^m x_3^n \quad a_{\ell,m,n} \in \mathbb{C} \right\}$$

For the basis functions $\boldsymbol{\varphi}_i$ generating the space $\mathbf{V}_h$, we use the basis functions detailed in Cohen and Duruflé (2007). For the basis functions $\boldsymbol{\psi}_i$ generating the space $\mathbf{W}_h$, we use Lagrange interpolation polynomial

$$\hat{\boldsymbol{\psi}}_{i_1,i_2,i_3,\ell}(\mathbf{x}) = \varphi_{i_1}^{\mathrm{GL}}(x_1)\varphi_{i_2}^{\mathrm{GL}}(x_2)\varphi_{i_3}^{\mathrm{GL}}(x_3)$$

where

$$\varphi_i^{\mathrm{GL}}(x) = \frac{\prod\limits_{j\neq i} x-\xi_j}{\prod\limits_{j\neq i} \xi_i-\xi_j}$$

with ξ_j the Gauss-Lobatto points on the interval $[0,1]$. The basis functions on the hexahedron K_i are then given as

$$\boldsymbol{\psi}_{i_1,i_2,i_3} \circ F_i = \hat{\boldsymbol{\psi}}_{i_1,i_2,i_3}$$

The stiffness and mass matrices $\mathbf{K}_h$ and $\mathbf{M}_h$ associated with the system (16) are given by:

$$\mathbf{M}_h = \begin{bmatrix} \mathbf{D}_h^E & 0 & 0 & 0 \\ 0 & \mu_b \mathbf{D}_h^H & 0 & 0 \\ 0 & 0 & \mathbf{D}_h & 0 \\ -\sigma_k \mathbf{C}_h^T & 0 & 0 & \mathbf{D}_h \end{bmatrix}$$

$$\mathbf{K}_h = \begin{bmatrix} \mathbf{S}_h & -\mathbf{R}_h & 0 & \mathbf{C}_h \\ \mathbf{R}_h^T & 0 & 0 & 0 \\ 0 & 0 & 0 & -\mathbf{D}_h \\ -c_k \mathbf{C}_h^T & 0 & \omega_{0,k}^2 \mathbf{D}_h & \gamma_k \mathbf{D}_h \end{bmatrix}$$

where h denotes the mesh size and

$$(\mathbf{D}_h^E)_{i,j} = \int_\Omega \varepsilon_e \, \boldsymbol{\varphi}_i(\mathbf{x}) \cdot \boldsymbol{\varphi}_j(\mathbf{x}) d\mathbf{x}$$

$$(\mathbf{D}_h)_{i,j} = \int_{\Omega_{res}} \boldsymbol{\varphi}_i(\mathbf{x}) \cdot \boldsymbol{\varphi}_j(\mathbf{x}) d\mathbf{x}$$

$$(\mathbf{D}_h^H)_{i,j} = \int_\Omega \boldsymbol{\psi}_i(\mathbf{x}) \cdot \boldsymbol{\psi}_j(\mathbf{x}) d\mathbf{x}$$

$$(\mathbf{C}_h)_{i,j} = \int_{\Omega_{res}} \boldsymbol{\varphi}_i(\mathbf{x}) \cdot \boldsymbol{\psi}_j(\mathbf{x}) d\mathbf{x}$$

$$(\mathbf{R}_h)_{i,j} = \int_\Omega \boldsymbol{\psi}_j(\mathbf{x}) \cdot \nabla \times \boldsymbol{\varphi}_i(\mathbf{x}) d\mathbf{x}$$

$$(\mathbf{S}_h)_{i,j} = \int_{\Gamma_S} \sqrt{\frac{\varepsilon_b}{\mu_b}} \, (\boldsymbol{\varphi}_i(\mathbf{x}) \times \mathbf{n}) \cdot (\boldsymbol{\varphi}_j(\mathbf{x}) \times \mathbf{n}) d\mathbf{x}$$

where $\mathbf{n}$ is the outgoing normale on the boundary Γ_S where a Silver-Müller condition can be set. Here, we consider

$$\varepsilon_e = \begin{cases} \varepsilon_\infty \text{ in } \Omega_{res} \\ \varepsilon_b, \text{ elsewhere.} \end{cases}$$

Degrees of freedom for $\mathbf{P}$ and $\mathbf{Q}$ are restricted to the domain Ω_{res}. All the integrals are evaluated with Gauss-Lobatto points such that matrices $\mathbf{D}_h$ and $\mathbf{D}_h^H$ are diagonal.

For the 2-D case, the unknown $\mathbf{E}$ is scalar (we consider the Transverse Electric case) and discretized with nodal continuous elements, unknowns $\mathbf{P}$ and $\mathbf{Q}$ are also scalar and discretized with basis functions of $\mathbf{E}$. The unknown $\mathbf{H}$ is vectorial and discretized with discontinuous elements. Basis functions are also based on Gauss-Lobatto to achieve mass lumping.

A.2 Second-order formulation

We use the same variational spaces and same basis functions as the previous section. The stiffness and mass matrices $\mathbf{K}_h$ and $\mathbf{M}_h$ associated with the system (26) are given by:

$$\mathbf{M}_h = \begin{bmatrix} \mathbf{D}_h^I & 0 & 0 & 0 \\ 0 & \mathbf{D}_h^E & 0 & 0 \\ 0 & 0 & \mathbf{D}_h & 0 \\ 0 & -\sigma_k \mathbf{C}_h^T & 0 & \mathbf{D}_h \end{bmatrix}$$

$$\mathbf{K}_h = \begin{bmatrix} 0 & -\mathbf{D}_h^I & 0 & 0 \\ \mathbf{K}_h^E & \mathbf{S}_h & 0 & \mathbf{C}_h \\ 0 & 0 & 0 & -\mathbf{D}_h \\ 0 & -c_k \mathbf{C}_h^T & \omega_{0,k}^2 \mathbf{D}_h & \gamma_k \mathbf{D}_h \end{bmatrix}$$

with the additional matrices

$$(\mathbf{D}_h^I)_{i,j} = \int_\Omega \boldsymbol{\varphi}_i(\mathbf{x}) \cdot \boldsymbol{\varphi}_j(\mathbf{x}) d\mathbf{x}$$

$$(\mathbf{K}_h^E)_{i,j} = \int_\Omega \frac{1}{\mu_b} \left(\nabla \times \boldsymbol{\varphi}_i(\mathbf{x})\right) \cdot \left(\nabla \times \boldsymbol{\varphi}_j(\mathbf{x})\right) d\mathbf{x}$$

B Computation of biorthogonal vector for 2-D PML

The proof of the relations given in subsection 4.6.1 is done with continuous operators $\mathbf{M}$ and $\mathbf{K}$. Its extension to discrete operators (i.e. matrices $\mathbf{M}_h$ and $\mathbf{K}_h$) is straightforward thanks to mass lumping. We have the eigenvalue problem:

$$\mathbf{K}\mathbf{x}_m = \lambda_m \mathbf{M}\mathbf{x}_m$$

where

$$\mathbf{x}_m = \begin{pmatrix} \tilde{u}_m \\ u_m^* \\ \mathbf{v}_m \end{pmatrix}$$

and

$$\mathbf{M} = \begin{pmatrix} \varepsilon_b & 0 & 0 \\ 0 & \varepsilon_b & 0 \\ 0 & 0 & -\mu_b \end{pmatrix}, \mathbf{K} = \begin{pmatrix} \varepsilon_b \left(\frac{\sigma_x + \sigma_y}{2}\right) & \varepsilon_b \left(\frac{\sigma_x - \sigma_y}{2}\right) & -\mathrm{div} \\ \varepsilon_b \left(\frac{\sigma_x - \sigma_y}{2}\right) & \varepsilon_b \left(\frac{\sigma_x + \sigma_y}{2}\right) & -\mathrm{div}_\perp \\ \nabla & 0 & -\mu_b \sigma \end{pmatrix}$$

where $\mathrm{div}_\perp v = \dfrac{\partial v_x}{\partial x} - \dfrac{\partial v_y}{\partial y}$ and $\nabla_\perp = \begin{vmatrix} \dfrac{\partial}{\partial x} \\ -\dfrac{\partial}{\partial y} \end{vmatrix}$ We want to know $\mathbf{x}_m^\perp$, the eigenvector of the adjoint problem:

$$\mathbf{K}^T \mathbf{x}_m^\perp = \lambda_m \mathbf{M}^T \mathbf{x}_m^\perp$$

where $\mathbf{x}_m^\perp$ is split into three components :

$$\mathbf{x}_m^\perp = \begin{pmatrix} u_m^\perp \\ u_m^{*,\perp} \\ \mathbf{v}_m^\perp \end{pmatrix}$$

We write the matrix $\mathbf{K}^T$ of the adjoint problem.

$$\mathbf{K}^T = \begin{pmatrix} \varepsilon_b\left(\frac{\sigma_x+\sigma_y}{2}\right) & \varepsilon_b\left(\frac{\sigma_x-\sigma_y}{2}\right) & -\mathrm{div} \\ \varepsilon_b\left(\frac{\sigma_x-\sigma_y}{2}\right) & \varepsilon_b\left(\frac{\sigma_x+\sigma_y}{2}\right) & 0 \\ \nabla & \nabla_\perp & -\mu_b\,\sigma \end{pmatrix}$$

The second equation of the adjoint problem yields a relation between $u_m^\perp$ and $u_m^{*,\perp}$:

$$\left(\frac{\sigma_x-\sigma_y}{2}\right) u_m^\perp + \left(\frac{\sigma_x+\sigma_y}{2}\right) u_m^{*,\perp} = \lambda_m u_m^{*,\perp}$$

We infer that

$$u_m^{*,\perp} = \frac{(\sigma_x-\sigma_y)u_m^\perp}{2\lambda_m-(\sigma_x+\sigma_y)}$$

The third equation gives us $\mathbf{v}_m^\perp$ as a function of $u_m^\perp$ and $u_m^{*,\perp}$

$$\mathbf{v}_m^\perp = \left[\mu_b\left(-\lambda_m+\sigma\right)\right]^{-1}\left(\nabla u_m^\perp + \nabla_\perp u_m^{*,\perp}\right).$$

The first equation of the adjoint eigenvalue problem is given as

$$\varepsilon_b\left(\frac{\sigma_x+\sigma_y}{2}\right) u_m^\perp + \varepsilon_b\left(\frac{\sigma_x-\sigma_y}{2}\right) u_m^{*,\perp} - \mathrm{div}\,\mathbf{v}_m^\perp = \lambda_m \varepsilon_b u_m^\perp$$

Using the two previous equations, we now get

$$\begin{aligned} &\varepsilon_b\left(\frac{\sigma_x+\sigma_y}{2}-\lambda_m\right) u_m^\perp + \varepsilon_b\left(\frac{\sigma_x-\sigma_y}{2}\right)^2 \frac{u_m^\perp}{\lambda_m - \dfrac{\sigma_x+\sigma_y}{2}} \\ &\quad - \mathrm{div}\left(\mu_b^{-1}(-\lambda_m+\sigma)^{-1}\left(\nabla u_m^\perp + \nabla_\perp\left(\frac{(\sigma_x-\sigma_y)u_m^\perp}{2\lambda-(\sigma_x+\sigma_y)}\right)\right)\right) = 0 \end{aligned}$$

and we denote y as

$$y = -\mathrm{div}\left(\mu_b^{-1}(-\lambda_m+\sigma)^{-1}\left(\nabla u_m^\perp + \nabla_\perp\left(\frac{(\sigma_x-\sigma_y)u_m^\perp}{2\lambda_m-(\sigma_x+\sigma_y)}\right)\right)\right)$$

The part of the variational formulation associated with y will provide

$$\begin{aligned} \int_\Omega y\,\varphi\,d\Omega \;=\; &\int_\Omega \frac{\mu_b^{-1}}{-\lambda_m+\sigma_x}\frac{\partial u_m^\perp}{\partial x}\frac{\partial \varphi}{\partial x} + \frac{\mu_b^{-1}}{-\lambda_m+\sigma_x}\frac{\partial}{\partial x}\left(\frac{\sigma_x-\sigma_y}{2\lambda_m-(\sigma_x+\sigma_y)}u_m^\perp\right)\frac{\partial\varphi}{\partial x} \\ &+\frac{\mu_b^{-1}}{-\lambda_m+\sigma_y}\frac{\partial u_m^\perp}{\partial y}\frac{\partial\varphi}{\partial y} - \frac{\mu_b^{-1}}{-\lambda_m+\sigma_y}\frac{\partial}{\partial y}\left(\frac{\sigma_x-\sigma_y}{2\lambda_m-(\sigma_x+\sigma_y)}u_m^\perp\right)\frac{\partial\varphi}{\partial y} \end{aligned}$$

Since the damping σ_y does not depend on x, we have

$$\frac{\partial}{\partial x}\left(\frac{2\lambda_m-(\sigma_x+\sigma_y)+(\sigma_x-\sigma_y)}{2\lambda_m-(\sigma_x+\sigma_y)}u_m^\perp\right) = 2(\lambda_m-\sigma_y)\frac{\partial}{\partial x}\left(\frac{u_m^\perp}{2\lambda_m-\sigma_x+\sigma_y}\right) = (-\lambda_m+\sigma_y)\frac{\partial u_m}{\partial x},$$

with

$$u_m = \frac{u_m^{\perp}}{-\lambda_m + \left(\dfrac{\sigma_x + \sigma_y}{2}\right)}.$$

Similarly, we proove

$$\frac{\partial}{\partial y}\left(\frac{2\lambda_m - (\sigma_x+\sigma_y) - (\sigma_x-\sigma_y)}{2\lambda - (\sigma_x+\sigma_y)} u_m^{\perp}\right) = (-\lambda_m + \sigma_x)\frac{\partial u_m}{\partial y}.$$

As a result, we obtain

$$\int_\Omega y\,\varphi\,d\Omega = \int_\Omega \mu_b^{-1}\left(\frac{-\lambda_m+\sigma_y}{-\lambda_m+\sigma_x}\right)\frac{\partial u_m}{\partial x}\frac{\partial \varphi}{\partial x} + \mu_b^{-1}\left(\frac{-\lambda_m+\sigma_x}{-\lambda_m+\sigma_y}\right)\frac{\partial u_m}{\partial y}\frac{\partial \varphi}{\partial y}\,d\Omega$$

For the mass terms, we have

$$\varepsilon_b\left[\left(-\lambda_m + \frac{\sigma_x+\sigma_y}{2}\right)^2 - \left(\frac{\sigma_x-\sigma_y}{2}\right)^2\right] u_m = \varepsilon_b(-\lambda_m+\sigma_x)(-\lambda_m+\sigma_y)u_m$$

Therefore, the unknown u_m satisfies the following variational formulation

$$\int_\Omega \varepsilon_b\,(-\lambda+\sigma_x)\,(-\lambda+\sigma_y)\,u_m\,\varphi + \mu_b^{-1}\begin{pmatrix} \dfrac{-\lambda+\sigma_y}{-\lambda+\sigma_x} & 0 \\ 0 & \dfrac{-\lambda+\sigma_x}{-\lambda+\sigma_y}\end{pmatrix}\nabla u_m\cdot\nabla\varphi\,d\Omega = 0$$

which is the same variational formulation satisfied by $\tilde{u}_m$ (first component of the eigenvector of $\mathbf{K}\mathbf{x}_m = \lambda_m\mathbf{M}\mathbf{x}_m$). u_m is proportional to $\tilde{u}_m$ if λ_m is a simple eigenvalue. In order to have $u_m^{\perp} = \tilde{u}_m$ in the physical domain, we will divide by $-\lambda_m$. We therefore have the following relation

$$u_m^{\perp} = \left(1 - \frac{\sigma_x+\sigma_y}{2\lambda_m}\right)\tilde{u}_m$$

We infer that

$$u_m^{*,\perp} = \frac{\sigma_x-\sigma_y}{2\lambda_m}\tilde{u}_m$$

For the last component $\mathbf{v}_m^{\perp}$, it is computed from $u_m^{\perp}$ and $u_m^{*,\perp}$

$$\mathbf{v}_m^{\perp} = \left|\begin{array}{l} \dfrac{\mu_b^{-1}}{-\lambda_m+\sigma_x}\left(\dfrac{\partial u_m^{\perp}}{\partial x} + \dfrac{\partial u_m^{*,\perp}}{\partial x}\right) \\ \dfrac{\mu_b^{-1}}{-\lambda_m+\sigma_y}\left(\dfrac{\partial u_m^{\perp}}{\partial y} - \dfrac{\partial u_m^{*,\perp}}{\partial y}\right)\end{array}\right.$$

C Computation of biorthogonal vector for 3-D PML

We have the eigenvalue problem

$$\mathbf{K}\mathbf{U} = \lambda_m\mathbf{M}\mathbf{U}$$

where $\lambda_m = i\tilde{\omega}_m$ is the eigenvalue with

$$\mathbf{M} = \begin{pmatrix} \varepsilon_b & 0 & 0 & 0 \\ 0 & \mu_b & 0 & 0 \\ -1 & 0 & 1 & 0 \\ 0 & -1 & 0 & 1 \end{pmatrix},\ \mathbf{K} = \begin{pmatrix} \varepsilon_b\mathbf{T}_{2,3,1} & 0 & 0 & -\nabla\times \\ 0 & \mu_b\mathbf{T}_{2,3,1} & \nabla\times & 0 \\ -\mathbf{T}_{1,2,3} & 0 & \mathbf{T}_{3,1,2} & 0 \\ 0 & -\mathbf{T}_{1,2,3} & 0 & \mathbf{T}_{3,1,2} \end{pmatrix},\ \mathbf{U} = \begin{pmatrix} \mathbf{E} \\ \mathbf{H} \\ \mathbf{E}^* \\ \mathbf{H}^* \end{pmatrix}$$

In order to find the left eigenvector of this system, we consider the adjoint eigenvalue problem to this system.

$$\mathbf{K}^T\mathbf{U}^\perp = \lambda\mathbf{M}^T\mathbf{U}^\perp,$$

with $\mathbf{U}^\perp = \left(\mathbf{E}^\perp, \mathbf{H}^\perp, \mathbf{E}^{*,\perp}, \mathbf{H}^{*,\perp}\right)$, which grants us the following system of equations:

$$\begin{cases} \varepsilon_b(-\lambda_m + \mathbf{T}_{2,3,1})\mathbf{E}^\perp - (-\lambda_m + \mathbf{T}_{1,2,3})\mathbf{E}^{*,\perp} = 0 \\ \mu_b(-\lambda_m + \mathbf{T}_{2,3,1})\mathbf{H}^\perp - (-\lambda_m + \mathbf{T}_{1,2,3})\mathbf{H}^{*,\perp} = 0 \\ (-\lambda_m + \mathbf{T}_{3,1,2})\mathbf{E}^{*,\perp} + \nabla\times\mathbf{H}^\perp = 0 \\ (-\lambda_m + \mathbf{T}_{3,1,2})\mathbf{H}^{*,\perp} - \nabla\times\mathbf{E}^\perp = 0 \end{cases} \tag{36}$$

We are now going to try to identify the different components of $\mathbf{U}^\perp$. First off we can show $\mathbf{E}^\perp = \mathbf{E}^*$. The third equation and second equation of (36) give:

$$\mathbf{E}^{*,\perp} = \frac{-\nabla\times\mathbf{H}^\perp}{-\lambda_m + \mathbf{T}_{3,1,2}} = \frac{-1}{-\lambda_m + \mathbf{T}_{3,1,2}}\nabla\times\left(\frac{-\lambda_m + \mathbf{T}_{1,2,3}}{\mu_b(-\lambda_m + \mathbf{T}_{2,3,1})}\mathbf{H}^{*,\perp}\right)$$

The first equation and fourth equation of (36), provide

$$\mathbf{E}^{*,\perp} = \frac{\varepsilon_b(-\lambda_m + \mathbf{T}_{2,3,1})}{-\lambda + \mathbf{T}_{1,2,3}}\mathbf{E}^\perp, \quad \mathbf{H}^{*,\perp} = \frac{\nabla\times\mathbf{E}^\perp}{-\lambda_m + \mathbf{T}_{3,1,2}}$$

By substituting these expressions in the previous equation, we obtain an equation in $\mathbf{E}^\perp$ only:

$$\frac{\varepsilon_b(-\lambda_m + \mathbf{T}_{2,3,1})}{-\lambda_m + \mathbf{T}_{1,2,3}}\mathbf{E}^\perp = \frac{-1}{-\lambda_m + \mathbf{T}_{3,1,2}}\nabla\times\left(-\frac{-\lambda_m + \mathbf{T}_{1,2,3}}{\mu_b(-\lambda_m + \mathbf{T}_{2,3,1})(-\lambda_m + \mathbf{T}_{3,1,2})}\nabla\times\mathbf{E}^\perp\right)$$

Since $\mathbf{E}^*$ verifies the same eigenvalue problem, we can choose the constant such that

$$\mathbf{E}^\perp = \mathbf{E}^*$$

Next, we will show that $\mathbf{H}^\perp = -\mathbf{H}^*$. Using $\mathbf{H}^{*,\perp} = \dfrac{\nabla\times\mathbf{E}^*}{-\lambda_m + \mathbf{T}_{3,1,2}}$ and $\mathbf{H}^{*,\perp} = \dfrac{\mu_b(-\lambda_m + \mathbf{T}_{2,3,1})}{-\lambda_m + \mathbf{T}_{1,2,3}}\mathbf{H}^\perp$, we can show that

$$\mathbf{H}^\perp = \frac{-\lambda_m + \mathbf{T}_{1,2,3}}{\mu_b(-\lambda_m + \mathbf{T}_{2,3,1})(-\lambda_m + \mathbf{T}_{3,1,2})}\nabla\times\mathbf{E}^* = -\mathbf{H}^*$$

and from there, it can easily be shown that

$$\mathbf{E}^{*,\perp} = \frac{-\lambda_m + \mathbf{T}_{2,3,1}}{-\lambda_m + \mathbf{T}_{3,1,2}}\,\varepsilon_b\,\mathbf{E}$$

$$\mathbf{H}^{*,\perp} = -\frac{-\lambda_m + \mathbf{T}_{2,3,1}}{-\lambda_m + \mathbf{T}_{3,1,2}}\,\mu_b\,\mathbf{H}$$

Which we can rewrite:

$$\mathbf{E}^{*,\perp} = \left(1 + \frac{\mathbf{T}_{2,3,1} - \mathbf{T}_{3,1,2}}{-\lambda_m + \mathbf{T}_{3,1,2}}\right)\varepsilon\mathbf{E}, \quad \mathbf{H}^{*,\perp} = -\left(1 + \frac{\mathbf{T}_{2,3,1} - \mathbf{T}_{3,1,2}}{-\lambda_m + \mathbf{T}_{3,1,2}}\right)\mu\mathbf{H},$$

Therefore we have obtained the left eigenvector given in formula (33).

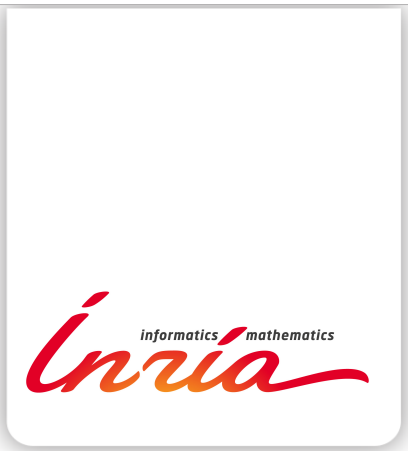

RESEARCH CENTRE
BORDEAUX – SUD-OUEST

200 avenue de la Vieille Tour
33405 Talence Cedex

Publisher
Inria
Domaine de Voluceau - Rocquencourt
BP 105 - 78153 Le Chesnay Cedex
inria.fr

ISSN 0249-6399